Article

SOURCE DATA | TRANSPARENT PROCESS

THE EMBO JOURNAL

Bicaudal-D1 regulates the intracellular sorting and signalling of neurotrophin receptors

Marco Terenzio[1,‡,†,**], Matthew Golding[1,§,†], Matthew R G Russell[2], Krzysztof B Wicher[3,¶], Ian Rosewell[4], Bradley Spencer-Dene[5], David Ish-Horowicz[3] & Giampietro Schiavo[1,6,*]

Abstract

We have identified a new function for the dynein adaptor Bicaudal D homolog 1 (BICD1) by screening a siRNA library for genes affecting the dynamics of neurotrophin receptor-containing endosomes in motor neurons (MNs). Depleting BICD1 increased the intracellular accumulation of brain-derived neurotrophic factor (BDNF)-activated TrkB and p75 neurotrophin receptor ($p75^{NTR}$) by disrupting the endosomal sorting, reducing lysosomal degradation and increasing the co-localisation of these neurotrophin receptors with retromer-associated sorting nexin 1. The resulting re-routing of active receptors increased their recycling to the plasma membrane and altered the repertoire of signalling-competent TrkB isoforms and $p75^{NTR}$ available for ligand binding on the neuronal surface. This resulted in attenuated, but more sustained, AKT activation in response to BDNF stimulation. These data, together with our observation that *Bicd1* expression is restricted to the developing nervous system when neurotrophin receptor expression peaks, indicate that BICD1 regulates neurotrophin signalling by modulating the endosomal sorting of internalised ligand-activated receptors.

Keywords Bicd1; intracellular sorting; neurotrophin signalling; p75NTR; TrkB

Subject Categories Membrane & Intracellular Transport; Neuroscience

DOI 10.15252/embj.201387579 | Received 3 December 2013 | Revised 14 March 2014 | Accepted 23 April 2014 | Published online 11 June 2014

The EMBO Journal (2014) 33: 1582–1598

Introduction

Neurons have complex axonal and dendritic arborisations, which are paramount for the function of the nervous system. The development and maturation of these extended neuronal networks require tight regulation of the intracellular transport of organelles and cargoes, such as mRNA, mitochondria, growth factor receptors and their signalling adaptor molecules, which in turn are necessary to ensure neuronal growth, differentiation and survival (Salinas *et al*, 2008; Hirokawa *et al*, 2010; Ascano *et al*, 2012).

Neurotrophins are essential for the development and maintenance of the nervous system (Ascano *et al*, 2012). The neurotrophin family consists of four structurally related growth factors: nerve growth factor (NGF), brain-derived neurotrophic factor (BDNF), NT3 and NT4/5 (Bibel & Barde, 2000; Huang & Reichardt, 2001). These ligands bind and activate the tropomyosin-related kinases TrkA, TrkB and TrkC either alone or in combination with p75 neurotrophin receptor ($p75^{NTR}$), which lacks enzymatic activity (Simi & Ibanez, 2010). Neurotrophin receptors have different binding specificities for their ligands: TrkA binds preferentially to NGF; TrkB to BDNF and NT4/5; and TrkC to NT-3, whilst $p75^{NTR}$ can bind all four neurotrophins, and their precursors, the pro-neurotrophins (Teng *et al*, 2010). The considerable crosstalk in the binding of neurotrophins to their receptors generates a variety of signalling outputs resulting in diverse cellular responses, which are initiated both by ligand availability and the relative abundance of each neurotrophin receptor at specific locations on the neuronal surface (Reichardt, 2006; Ascano *et al*, 2012). This signalling diversity is further enhanced because the same neurotrophin can have opposing effects, depending on whether it is presented to the neuron as the precursor or mature form (Teng *et al*, 2010). It is therefore important that neurotrophin signalling is tightly controlled both spatially and temporally, particularly in the developing nervous system when neurotrophins and their receptors are abundantly expressed.

The signalling cascades activated by neurotrophins in the neuronal periphery are regulated by the endocytosis, sorting and trafficking of neurotrophin receptors along the axon or dendrites

1 Molecular NeuroPathobiology Laboratory, Cancer Research UK London Research Institute, London, UK
2 Electron Microscopy Laboratory, Cancer Research UK London Research Institute, London, UK
3 Developmental Genetics Laboratory, Cancer Research UK London Research Institute, London, UK
4 Transgenic Services laboratory, Cancer Research UK London Research Institute, London, UK
5 Experimental Histopathology Laboratory, Cancer Research UK London Research Institute, London, UK
6 Sobell Department of Motor Neuroscience & Movement Disorders, UCL-Institute of Neurology, University College London, London, UK
*Corresponding author. Tel: +44 7918 738393; Fax: +44 20 7813 3107; E-mail: giampietro.schiavo@ucl.ac.uk
**Corresponding author. Tel: +972 8934 4265; Fax: +972 8934 4112; E-mail: marco.terenzio@weizmann.ac.il
†Contributed equally to this work
‡Present address: Department of Biological Chemistry, Weizmann Institute of Science, Rehovot, Israel
§Present address: Centre for Microvascular Research, William Harvey Research Institute, Barts & The London School of Medicine and Dentistry, Queen Mary University of London, London, UK
¶Present address: Medimmune, Department of Antibody Discovery and Protein Engineering, Cambridge, UK

towards the cell body, where they elicit transcriptional responses (Ibanez, 2007; Ascano *et al*, 2012; Schmieg *et al*, 2014). We have previously shown that the binding fragment of tetanus neurotoxin (H_CT) is a reliable probe to monitor neurotrophin receptor uptake and intracellular trafficking (Bercsenyi *et al*, 2013). Indeed, H_CT and $p75^{NTR}$ bound to NGF accumulate in clathrin-coated pits and are internalised by a clathrin-mediated endocytic pathway in motor neurons (MNs) (Deinhardt *et al*, 2006a, 2007). Furthermore, H_CT shares the same axonal retrograde transport organelles with neurotrophins and their receptors (Lalli & Schiavo, 2002; Deinhardt *et al*, 2006b).

Since a comprehensive understanding of the molecular mechanisms controlling neurotrophin receptor internalisation and trafficking is still lacking, we sought to identify new genes involved in this pathway by performing an small interfering RNA (siRNA) screen in MNs derived from transgenic HB9-GFP embryonic stem (ES) cells using H_CT and an antibody directed against the extracellular domain of $p75^{NTR}$ ($\alpha p75^{NTR}$) as fluorescent reporters (Terenzio *et al*, 2014). Importantly, expression of green fluorescent protein (GFP) driven by the Hb9 homeobox gene enhancer (Wichterle *et al*, 2002) facilitated the unequivocal identification of MNs generated from these ES cells upon differentiation (Terenzio *et al*, 2014).

Using this approach, we identified a small cohort of genes affecting the intracellular accumulation of H_CT and $\alpha p75^{NTR}$ when silenced (see Supplementary Table S1). Knockdown of one gene in particular, *Bicaudal D homolog 1* (*Bicd1*), revealed an increased internalisation phenotype for H_CT and was selected for further analyses, which demonstrated that BICD1 depletion also increased the intracellular accumulation of ligand-bound $p75^{NTR}$ and TrkB (Terenzio *et al*, 2014).

Bicaudal D homolog 1 is known to participate in endosomal trafficking and dynein-mediated processes (Hoogenraad *et al*, 2001; Matanis *et al*, 2002; Bianco *et al*, 2010; Aguirre-Chen *et al*, 2011), including retrograde transport in neuronal cells (Wanschers *et al*, 2007). Furthermore, BICD1 has important roles in the development and function of the *Drosophila* and *Caenorhabditis elegans* nervous systems (Li *et al*, 2010). We now show that BICD1 is a key regulator of the intracellular trafficking of neurotrophin receptors and that it performs this role by controlling the BDNF-triggered sorting and progression of $p75^{NTR}$ and TrkB through the endosomal pathway. Thus, BICD1 depletion disrupted this mechanism to favour $p75^{NTR}$ and TrkB recycling over lysosomal degradation, which in turn affected signalling responses to BDNF stimulation.

Our data identify a novel function for BICD1 as a modulator of neurotrophin receptor dynamics and signalling, which may also be relevant for other receptor tyrosine kinases in different cellular systems.

Results

Bicd1 is strongly expressed in the developing central and peripheral nervous systems

One of the most prominent candidates from our siRNA screen was BICD1 (Terenzio *et al*, 2014). Since BICD1 and related proteins are cytoplasmic dynein adaptors (Hoogenraad *et al*, 2001; Matanis *et al*, 2002), and BICD1 has been postulated to function in retrograde transport (Wanschers *et al*, 2007), we decided to focus our efforts on addressing the role played by BICD1 in the regulation of neurotrophin receptor trafficking in our model system.

We used a *Bicd1* gene-trapped ES cell clone ($Bicd1^{gt/+}$; gene trap RRP227) for the functional characterisation of BICD1. This gene trap vector expressed a β-galactosidase cassette, allowing us to determine *Bicd1* expression patterns in chimeric embryos generated from $Bicd1^{gt/+}$ ES cells (Fig 1A). X-gal histochemistry of $Bicd1^{gt/+}$ ES cell-derived embryos revealed that at embryonic day 12 (E12), *Bicd1* was highly and almost exclusively expressed in ventral horn MNs of the developing spinal cord (Fig 1A′–A‴), dorsal root ganglia (DRG; Fig 1A″–A‴) and brain (Fig 1A′ and A″). These X-gal-stained embryos were then paraffin embedded, cross-sectioned and immunostained to reveal that *Bicd1* expression was highest in HB9-positive ventral horn MNs (Fig 1B), a sub-population of DRG neurons (Fig 1D) and in the nerve tracts emanating from these structures (Fig 1A‴,C). High *Bicd1* expression in the developing nervous tissue closely matched the pattern of immunoreactivity for BDNF, Trk receptors and $p75^{NTR}$ (Supplementary Fig S1A–C). Altogether, these observations suggest that BICD1 plays a role in the developing nervous system at a time when neurotrophins and their receptors are highly expressed (Davies, 1994; Klein, 1994; Ernfors, 2001).

However, only one developmental day later, the expression pattern of *Bicd1* had dramatically changed: at E14.5, *Bicd1*-LacZ had been lost from the brain (Supplementary Fig S1E) and spinal cord (Supplementary Fig S1F), yet was still strongly retained in DRG (Supplementary Fig S1F and G) and was most notably upregulated in skin, skeletal muscle and heart ventricles, but interestingly, not in the atria (Supplementary Fig S1H).

$Bicd1^{gt/gt}$ ES-cell-derived MNs are a reliable *in vitro* model system to study BICD1 function

We had planned to use $Bicd1^{gt/+}$ × C57/Bl6 mouse chimeras to generate a $Bicd1^{gt/+}$ founder colony. However, mating of male chimeras with approximately 75% ES cell contribution to wild-type females produced no mutant offspring, indicating that germline transmission of the $Bicd1^{gt/+}$ allele had failed to take place. We therefore selected for loss of heterozygosity in culture using high G418 concentrations (Lefebvre *et al*, 2001). Resultant homozygous $Bicd1^{gt/gt}$ ES cells were isolated, expanded and differentiated into MNs.

BICD1 transcript and protein levels were reduced by approximately 70% in $Bicd1^{gt/gt}$ MNs compared to wild-type cells (Fig 1E and F; Supplementary Fig S1D). Complete ablation of *Bicd1* expression was not expected since gene trap insertions are prone to unpredicted downstream mRNA splicing events (Voss *et al*, 1998). In contrast, *Bicd2* mRNA levels were found to be approximately 80% higher in $Bicd1^{gt/gt}$ MNs compared to wild-type controls (Supplementary Fig S1D), suggesting that BICD2 might compensate for the partial loss of BICD1. However, this scenario is unlikely since BICD2 protein levels were not increased in $Bicd1^{gt/gt}$ MNs (Supplementary Fig S2A).

BICD1 depletion had no significant effect on the expression of the MN markers *Hb9* and *ChAT* (choline acetyltransferase; Supplementary Fig S1D), or $p75^{NTR}$ (Fig 1E and F; Supplementary Fig S1D), whilst Trk protein levels showed an approximate 30% decrease using a pan-Trk antibody (Fig 1F). Since MNs do not

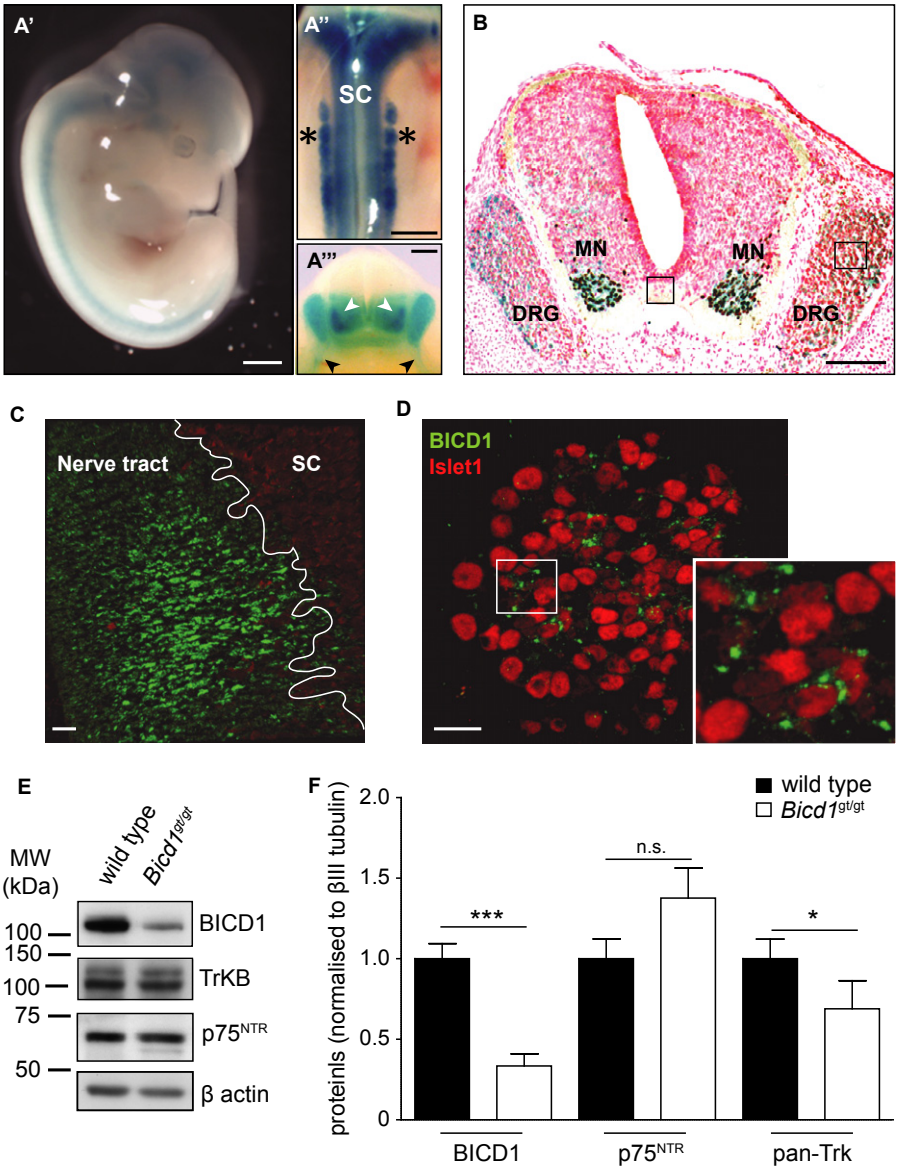

Figure 1. Validation of *Bicaudal D homolog 1* (*Bicd1*) gene-trapped embryonic stem (ES) cells.

A Lateral (A') and dorsal (A'') views of an X-gal-stained E12.5 embryo derived from RRP227 *Bicd1*$^{gt/+}$ ES cells, demonstrating *Bicd1* expression throughout the developing nervous system, but particularly strong in the spinal cord (SC), hindbrain and dorsal root ganglia (DRG, asterisks). Scale bars, 1 mm. Removing the head at the cervical region and visualising the cut surface (A''') shows that *Bicd1* expression is particularly high in the ventral horns of the spinal cord (white arrowheads), DRG and ventral nerve tracts descending from these structures (black arrowheads). Scale bar, 200 μm.

B Paraffin-embedded transverse section taken from the thoracic region of the embryo shown in (A), immunostained for HB9 and counterstained with Nile red. HB9 protein (brown) is localised exclusively in ventral horn motor neuron nuclei (MN), whilst *Bicd1*-lacZ (blue) is expressed both in MNs and adjacent DRG. Scale bar, 100 μm.

C, D Transverse section of a spinal cord of a E12.5 wild-type mouse embryo immunostained for BICD1 (green) and Islet1 (red). Images taken from regions approximated by the black boxes in (B) show intense immunoreactivity for BICD1 in nerve tracts (C; central box in B) and in a subset of Islet1-positive DRG nuclei (D; right side box in B). Scale bars, 20 μm.

E Western blotting of whole-cell lysates generated from *Bicd1*$^{gt/gt}$ and wild-type control ES cell-derived MNs showing relative expression levels of BICD1, TrkB, p75^{NTR} and β-actin as a loading control.

F Quantification of western blots for BICD1, pan-Trk (correspondent to TrkB and TrkC receptors in these samples) and p75^{NTR} normalised to βIII tubulin (n = 3, paired t-test, mean ± s.e.m., *P < 0.05, ***P < 0.001; n.s., not significant).

Source data are available online for this figure.

express TrkA, this reduction could only be attributed to decreased levels of TrkB and/or TrkC. Accordingly, a similar decrease of TrkB transcript levels was observed (Supplementary Fig S1D).

Importantly, *Bicd1*$^{gt/gt}$ MNs were indistinguishable from their wild-type counterparts, since we observed no statistically significant difference in terms of either the abundance of synaptic

boutons (Supplementary Fig S2B and C) or the morphology of the neurite network (Supplementary Fig S2D–G). Taken together, these results demonstrated that RRP227 gene trap ES-cell-derived MNs were a suitable model system with which to investigate the functional consequences of BICD1 depletion on the trafficking of neurotrophin receptors.

BICD1 depletion affects the internalisation and intracellular fate of H_CT

Our siRNA screen revealed that *Bicd1* knockdown increased the intracellular accumulation of H_CT compared to cells transfected with control siRNA (Terenzio *et al*, 2014), a phenotype that was replicated in *Bicd1*$^{gt/gt}$ MNs (Fig 2A and B). Overexpressing BICD1-GFP in *Bicd1*$^{gt/gt}$ MNs rescued this phenotype by decreasing H_CT accumulation compared to neurons expressing GFP alone (Fig 2C and Supplementary Fig S3A), confirming that the observed phenotype was a direct consequence of BICD1 depletion. To further investigate the nature of the intracellular compartment to which BICD1 associates, we purified a population of endosomes containing monocrystalline ion oxide nanoparticles (MION)-conjugated H_CT (Deinhardt *et al*, 2006b; Wade *et al*, 2012). Many of these organelles are signalling endosomes as they are known to contain Trk receptors and p75^{NTR} and are transported from the periphery towards the MN soma by cytoplasmic dynein (Schmieg *et al*, 2014). BICD1 associated with this compartment together with its known interactors p150^{Glued} and p50, two subunits of the dynactin complex that are required for dynein motor activity, and Rab6, a small GTPase involved in Golgi to ER retrograde trafficking (Supplementary Fig S3B; Matanis *et al*, 2002; Fuchs *et al*, 2005).

Because BICD1 undergoes axonal retrograde transport (Terenzio *et al*, 2014) and has been previously implicated in regulating this dynein mediated process (Wanschers *et al*, 2007), we tested whether this trafficking pathway was altered in *Bicd1*$^{gt/gt}$ MNs. Surprisingly, there was no significant difference in the speed or frequency of axonal retrograde carriers containing αp75^{NTR} (Supplementary Fig S3C) or H_CT (Terenzio *et al*, 2014) between wild-type and mutant neurons, suggesting that the increase in somatic accumulation of H_CT observed in MNs depleted of BICD1 was not due to abnormalities in axonal retrograde transport.

Alternatively, the increased accumulation of H_CT in *Bicd1*$^{gt/gt}$ MNs (Fig 2A and B) might have been caused by defective endosomal sorting and/or trafficking of this probe in the cell soma. To test this possibility, we used transmission electron microscopy to trace the intracellular fate of internalised colloidal gold-conjugated H_CT in wild-type and *Bicd1*$^{gt/gt}$ MNs and determined the morphology of gold-containing organelles at the ultrastructural level (Figs 2D and 4). Some of these H_CT-containing compartments resembled multivesicular bodies (MVBs), which was not surprising since H_CT was previously reported to associate with these organelles (Parton *et al*, 1987). Other H_CT-containing membrane compartments were described on the basis of their contents: 'amorphous' (no clearly identifiable content and low electron density), 'membranous' (relatively high membrane content) and 'tubular', because of their characteristic morphology (Fig 2D). Compared to wild-type cells, *Bicd1*$^{gt/gt}$ MNs contained significantly more H_CT in the 'amorphous' compartments where it clustered close to the limiting membrane (Fig 2D). Interestingly, when compared to wild-type controls, *Bicd1*$^{gt/gt}$ MNs displayed an inverse relationship in the abundance of H_CT-positive 'amorphous' organelles relative to MVBs (Fig 2E). Occasionally, H_CT concentrated as clusters within bud-like protrusions, which were often contiguous with the lumen of compartments with 'amorphous content' (Supplementary Fig S3D). These structures were more commonly observed in *Bicd1*$^{gt/gt}$ MNs and we believe that they represent enlarged endosomal sorting compartments.

TrkB associates with enlarged endosomal compartments in *Bicd1*$^{gt/gt}$ MNs

Because H_CT displayed an extensive co-localisation with TrkB (Fig 3A) and p75^{NTR} (Lalli & Schiavo, 2002; Deinhardt *et al*, 2006b, 2007) in wild-type MNs, we inferred that neurotrophin receptors may also associate with enlarged endosomes in BICD1-depleted cells. Electron microscopy of wild-type and *Bicd1*$^{gt/gt}$ MNs incubated for 2 h with a cocktail of colloidal gold-labelled probes: H_CT (10 nm) together with antibodies directed against TrkB (20 nm) and p75^{NTR} (5 nm) demonstrated that neurotrophin receptors and H_CT were all present within a sub-population of endosomes (Fig 4). As expected, the accumulation of all three probes within these organelles was greater in *Bicd1*$^{gt/gt}$ MNs compared to wild-type cells (compare Fig 4A with 4B), indicating that endosomal trafficking of neurotrophin receptors was also affected by BICD1 depletion.

The increased association of H_CT, TrkB and p75^{NTR} with these compartments in *Bicd1*$^{gt/gt}$ MNs suggested that BICD1 could play a role in the endocytic sorting of neurotrophin receptors and H_CT in neuronal cell bodies. This view was supported by observations that H_CT co-localised with components of the retromer complex, most notably sorting nexin 1 (SNX1; Supplementary Fig S4A and B) and Vps26 (Terenzio *et al*, 2014). TrkB was also localised to endogenous SNX1-positive compartments (Fig 3B and C). We used N2A neuroblastoma cells overexpressing FLAG-tagged TrkB for this experiment because of the inability to simultaneously detect endogenous TrkB and SNX1 using antibodies raised in the same species (see Supplementary Information). Furthermore, FLAG-TrkB overexpression in N2A cells followed by incubation with BDNF-mCherry demonstrated that endogenous BICD1 co-localised with BDNF/TrkB-positive organelles (Fig 3D).

Importantly, the co-distribution of H_CT with SNX1-positive compartments was higher in *Bicd1*$^{gt/gt}$ MNs compared to wild-type cells (Supplementary Fig S4A and B), suggesting that SNX1-dependent sorting of H_CT and neurotrophin receptors was affected by BICD1 depletion.

BICD1 depletion enhances the neurotrophin-dependent intracellular accumulation of p75^{NTR} and TrkB

We previously showed that p75^{NTR} undergoes rapid recycling at the plasma membrane in the absence of neurotrophins (Deinhardt *et al*, 2007). This steady-state recycling of p75^{NTR} in the absence of exogenous ligands was unaffected by BICD1 depletion (Supplementary Fig S5A and B). To test whether BICD1 was required for the BDNF-induced trafficking of p75^{NTR}, we treated wild-type and *Bicd1*$^{gt/gt}$ MNs with exogenous BDNF, a treatment which promotes the recruitment of p75^{NTR} to a clathrin-dependent endocytic pathway linked to axonal retrograde transport (Deinhardt *et al*, 2007). The

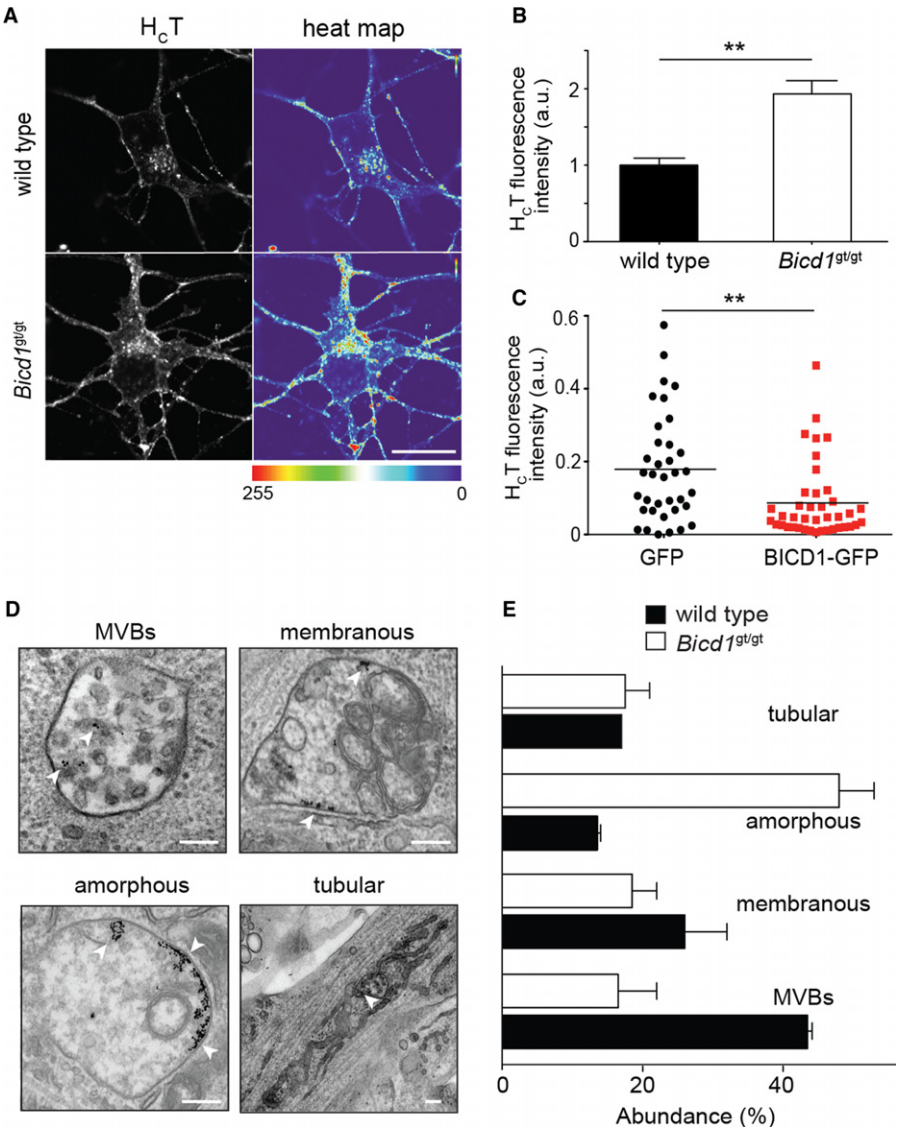

Figure 2. Internalisation of the binding fragment of tetanus toxin (H$_C$T) in *Bicd1*$^{gt/gt}$ motor neurons (MNs).

A, B AlexaFluor555-conjugated H$_C$T was internalised for 1 h at 37°C by wild-type and *Bicd1*$^{gt/gt}$ MNs, which were then acid-washed and fixed. (A) Representative pseudo-coloured images of wild-type (top) and *Bicd1*$^{gt/gt}$ (bottom) MNs were used to generate a heat map profile to better visualise the difference in relative amounts of internalised H$_C$T between the two genotypes. Scale bar, 20 μm. (B) Quantification of H$_C$T internalised by wild-type and *Bicd1*$^{gt/gt}$ MNs after 1 h incubation at 37°C (n = 3, t-test, mean ± s.e.m., $^{**}P < 0.01$).

C Quantification of H$_C$T internalised by *Bicd1*$^{gt/gt}$ MNs overexpressing GFP or BICD-GFP for 1 h at 37°C. Note that BICD1-GFP overexpression significantly decreased H$_C$T accumulation (red squares; 35–40 transfected cells were quantified per genotype; Mann–Whitney test, $^{**}P < 0.01$).

D Gold-conjugated H$_C$T (10 nm) was internalised for 1 h at 37°C by wild-type and *Bicd1*$^{gt/gt}$ MNs, which were then fixed and processed for transmission electron microscopy. In *Bicd1*$^{gt/gt}$ MNs, colloidal gold-H$_C$T (arrowheads) accumulated in different types of organelles, which were classified as MVBs, endosomes containing membranes ('membranous'), endosomes with amorphous content ('amorphous') and tubular endosomes ('tubular'). Scale bar, 200 nm.

E Quantification of the relative abundance of each sub-type of colloidal gold-H$_C$T-containing organelle for each genotype (n = 2, mean ± s.e.m.).

addition of BDNF resulted in a marked increase in the intracellular accumulation of αp75^{NTR}, which was significantly higher in *Bicd1*$^{gt/gt}$ MNs compared to wild-type controls (Supplementary Fig S5C and D), indicating that BICD1 is required for the trafficking of BDNF-bound p75^{NTR}, but does not influence the neurotrophin-independent trafficking of this receptor. This effect was unlikely to have resulted from any alteration in the axonal retrograde transport of αp75^{NTR}, as this process was not affected by BICD1 depletion (Supplementary Fig S3C).

A similar ligand-dependent accumulation phenotype was also observed for TrkB in *Bicd1*$^{gt/gt}$ MNs (Fig 5A and D). Like many receptor tyrosine kinases, activated TrkB-BDNF complexes traffic to the late endosomal pathway and are ultimately delivered to lysosomes for degradation (Chen *et al*, 2005). We tested whether the increased accumulation of ligand-activated TrkB in *Bicd1*$^{gt/gt}$ MNs was caused by the defective sorting of antibody-bound TrkB to lysosomes, by inhibiting lysosomal proteases using a cocktail of well-characterised inhibitors (leupeptin, E64D and pepstatin A). Under

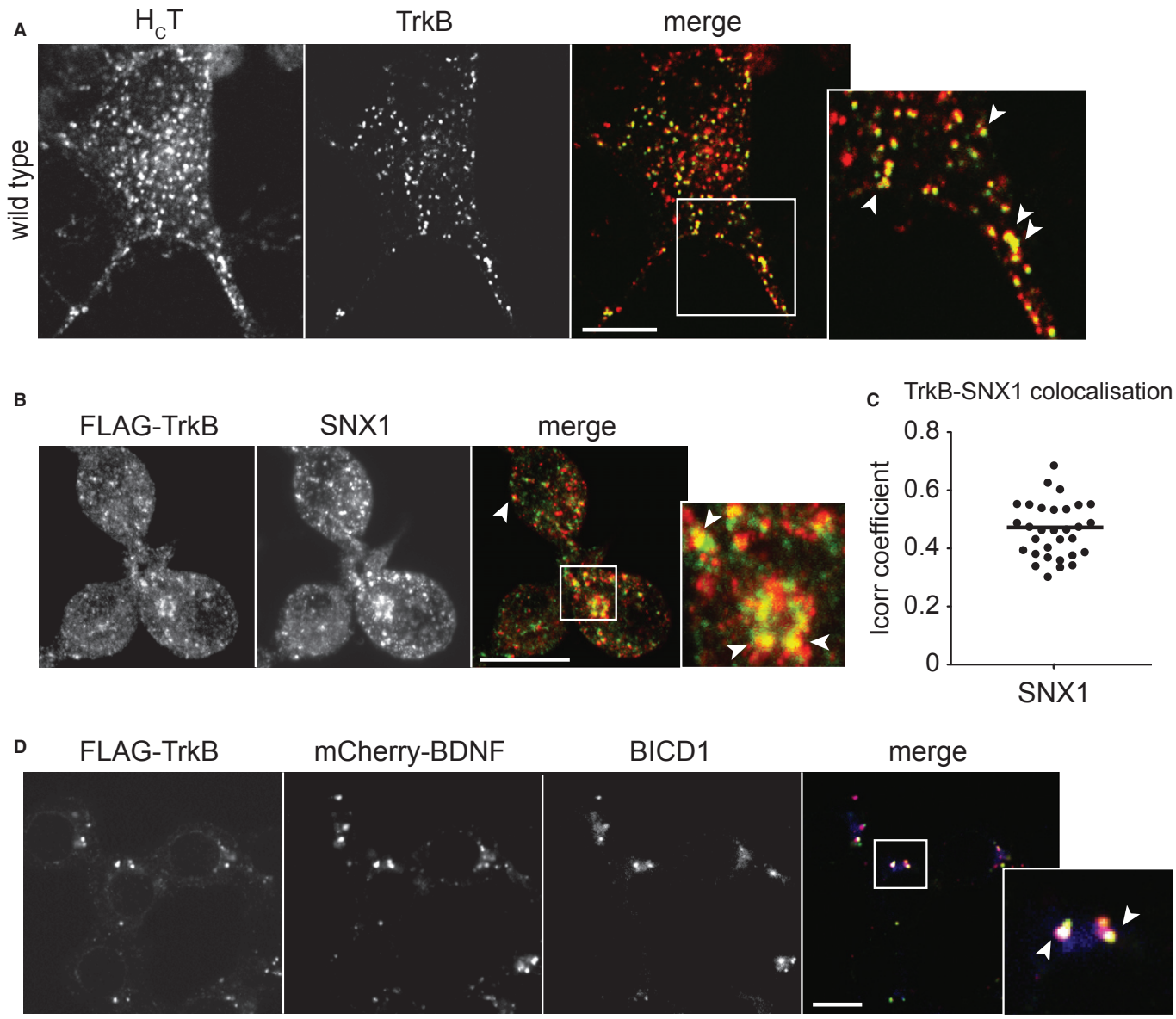

Figure 3. Sorting nexin 1 (SNX1) co-localises with TrkB and the binding fragment of tetanus toxin (H_CT).

A H_CT and TrkB co-localise in wild-type motor neurons (MNs). AlexaFluor555-conjugated H_CT (red) was internalised for 1 h at 37°C; neurons were then acid-washed, fixed and immunostained for TrkB (green). TrkB/H_CT-positive structures (arrowheads) were frequently detected in the cell soma and neurites. Scale bar, 5 μm.

B N2A neuroblastoma cells over-expressing FLAG-TrkB were incubated with FLAG antibody and brain-derived neurotrophic factor (BDNF) for 1 h at 37°C and then acid-washed, fixed and immunostained to detect FLAG-TrkB (green) and endogenous SNX1 (red). Scale bar, 10 μm.

C Quantification of FLAG-TrkB/SNX1 co-localisation (n = 3, 31 cells in total analysed).

D N2A cells overexpressing FLAG-TrkB were incubated with FLAG antibody and BDNF-mCherry (red) for 1 h at 37°C and then acid-washed, fixed and immunostained to detect FLAG-TrkB (green) and endogenous Bicaudal D homolog 1 (BICD1) (blue). Note the presence of triple positive structures demonstrating that endogenous BICD1 associates with internalised TrkB-BDNF complexes. Scale bar, 10 μm.

these conditions, TrkB accumulation was increased in wild-type MNs, whereas the extent of TrkB accumulation in *Bicd1*$^{gt/gt}$ MNs was unaffected by this treatment (Supplementary Fig S6A). A similar trend was also established for αp75^{NTR} accumulation (Supplementary Fig S6B). We did not detect any obvious difference either in lysosomal acidification or distribution of LAMP2-positive organelles between *Bicd1*$^{gt/gt}$ and wild-type MNs, suggesting that BICD1 depletion does not affect lysosome biogenesis or function, but is likely to cause an impaired sorting of neurotrophin receptors along the degradative pathway. Consistent with this idea was our observation that intracellular accumulation of H_CT was unaffected by lysosomal inhibitors (Supplementary Fig S6C), which was not surprising since this probe does not enter the lumen of lysosomes (Supplementary Fig S6D) and therefore is not degraded by these organelles.

Since the results described in Supplementary Fig S6A and B were obtained by an imaging approach using fluorescent αTrkB and

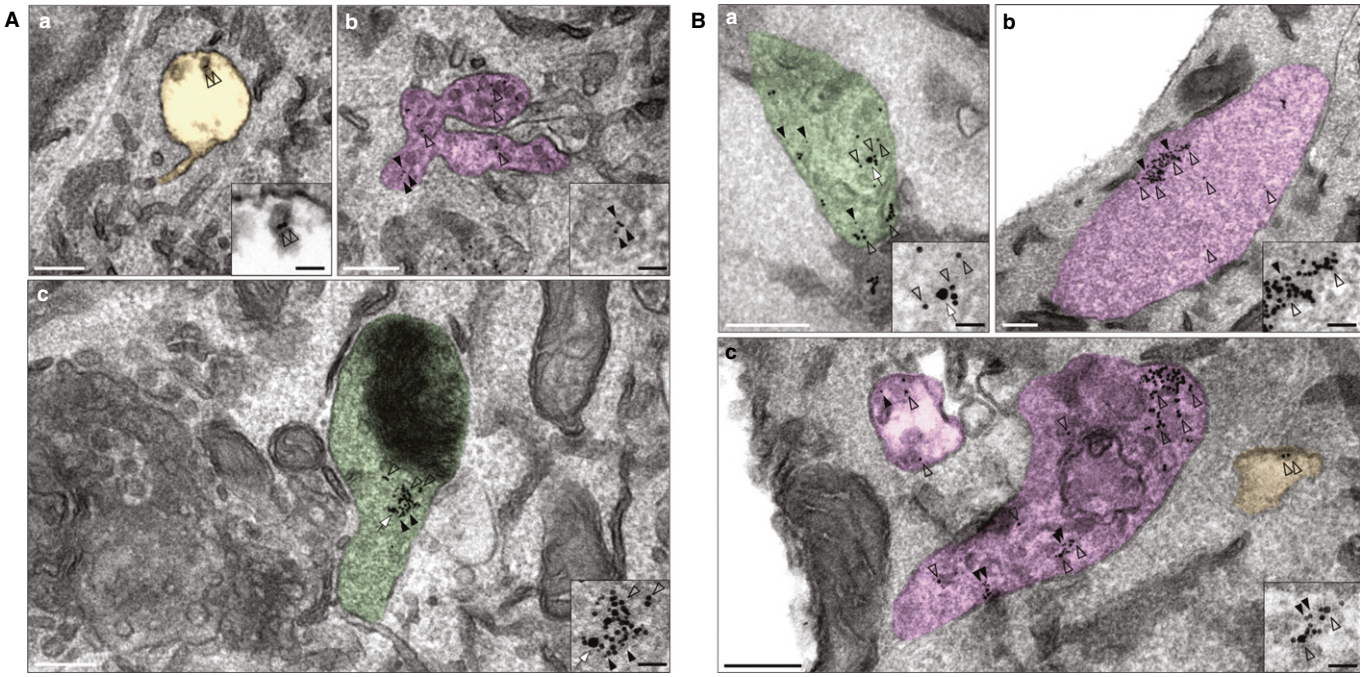

Figure 4. *Bicd1*$^{gt/gt}$ motor neurons accumulate H_CT, TrkB and p75^{NTR} in enlarged endosomal structures.

A Wild-type MNs were allowed to internalise gold-conjugated H_CT (10 nm, empty arrowheads), αTrkB (20 nm, white arrowheads) and αp75^{NTR} (5 nm, black arrowheads) in the presence of BDNF for 2 h at 37°C and then processed for transmission electron microscopy. Colloidal gold-conjugated probes were found in a variety of organelles ranging from tubular endosomes (Aa), to MVBs (Ab, Bc) to endosomes containing membranes (Ac). These organelles are pseudocoloured according to the number of probes that they contain: yellow, pink and green representing single, double and triple labelled compartments, respectively. Scale bars, 200 nm (main panels); 50 nm (insets).

B *Bicd1*$^{gt/gt}$ MNs were treated as in (A) and then processed for transmission electron microscopy. Notably, in addition to the previously described organelles, colloidal gold-conjugated probes were strongly associated with endosomes with "amorphous" content (Ba, Bb). In addition, double and triple labelled enlarged organelles were more prevalent in *Bicd1*$^{gt/gt}$ motor neurons compared to wild-type cells. Scale bars, 200 nm (main panels); 50 nm (insets).

αp75^{NTR}, we wanted to confirm these results using a more direct biochemical strategy. For this purpose, we selected a pulse-chase protocol, which allowed us to follow the dynamics of a cohort of internalised receptors as they trafficked along the endosomal pathway. To this end, we loaded ES-derived MNs with a 15-min pulse of αTrkB in the presence of BDNF and lysosomal inhibitors or vehicle control, followed by 1 or 2 h incubation in the presence or absence of lysosomal inhibitors. After cell lysis, antibody pulldown followed by western blotting revealed a major band of full-length TrkB (TrkB.FL; 145 kDa) and a minor band of TrkB.T1 (90 kDa), representing the truncated dominant-negative form of this receptor (Fenner, 2012), in wild-type cells (upper panel, Fig 5E). However, samples isolated from *Bicd1*$^{gt/gt}$ MNs displayed a striking increase of TrkB.T1 relative to TrkB.FL (lower panel, Fig 5E). In agreement with the immunofluorescence data quantified in Supplementary Fig S6A, lysosomal inhibitors proved effective in preventing the degradation of αTrkB in wild-type, but not in *Bicd1*$^{gt/gt}$ MNs (Fig 5E), suggesting that BICD1 depletion impaired lysosome-mediated degradation of these receptors.

TrkA is degraded by the combined actions of lysosomes and the proteasome (Sommerfeld *et al*, 2000; Geetha & Wooten, 2008), a pathway shared at least in part by TrkB (Sommerfeld *et al*, 2000). Interestingly, proteasomal inhibition redirects TrkA from late endosomes to the recycling route (Moises *et al*, 2009). Therefore, the residual degradation of TrkB by wild-type MNs in the presence of lysosomal protease inhibitors at the latest time point (Fig 5E, 120 min) could have resulted from receptor clearance by the proteasome and suggested a possible explanation for the apparent ineffectiveness of lysosomal inhibitors in preventing the clearance of TrkB from *Bicd1*$^{gt/gt}$ MNs (lower panel, Fig 5E). To test this hypothesis and assess the impact of BICD1 on these degradative pathways, we repeated the 15-min pulse step in the presence or absence of MG132, a specific proteasome inhibitor. Thus, probing the αTrkB immunoprecipitates with a TrkB antibody revealed profiles similar to those shown in the previous experiment (compare upper panels in Fig 5F with 5E). However, re-probing the same membrane with a ubiquitin-specific antibody revealed a signal only for the *Bicd1*$^{gt/gt}$ sample treated with a combination of lysosomal inhibitors and MG132 (Fig 5F). This result implied that within 15 min of exposure to BDNF, TrkB internalised by *Bicd1*$^{gt/gt}$ MNs was preferentially ubiquitinated and likely targeted for proteasome-mediated degradation.

BICD1 depletion increases neurotrophin receptor levels at the plasma membrane

Inhibition of the proteasome, which causes an accumulation of ubiquitinated Trks, redirects TrkA from late endosomes to a plasma membrane recycling pathway (Moises *et al*, 2009). Depletion of BICD1 on the other hand led to the intracellular increase of H_CT,

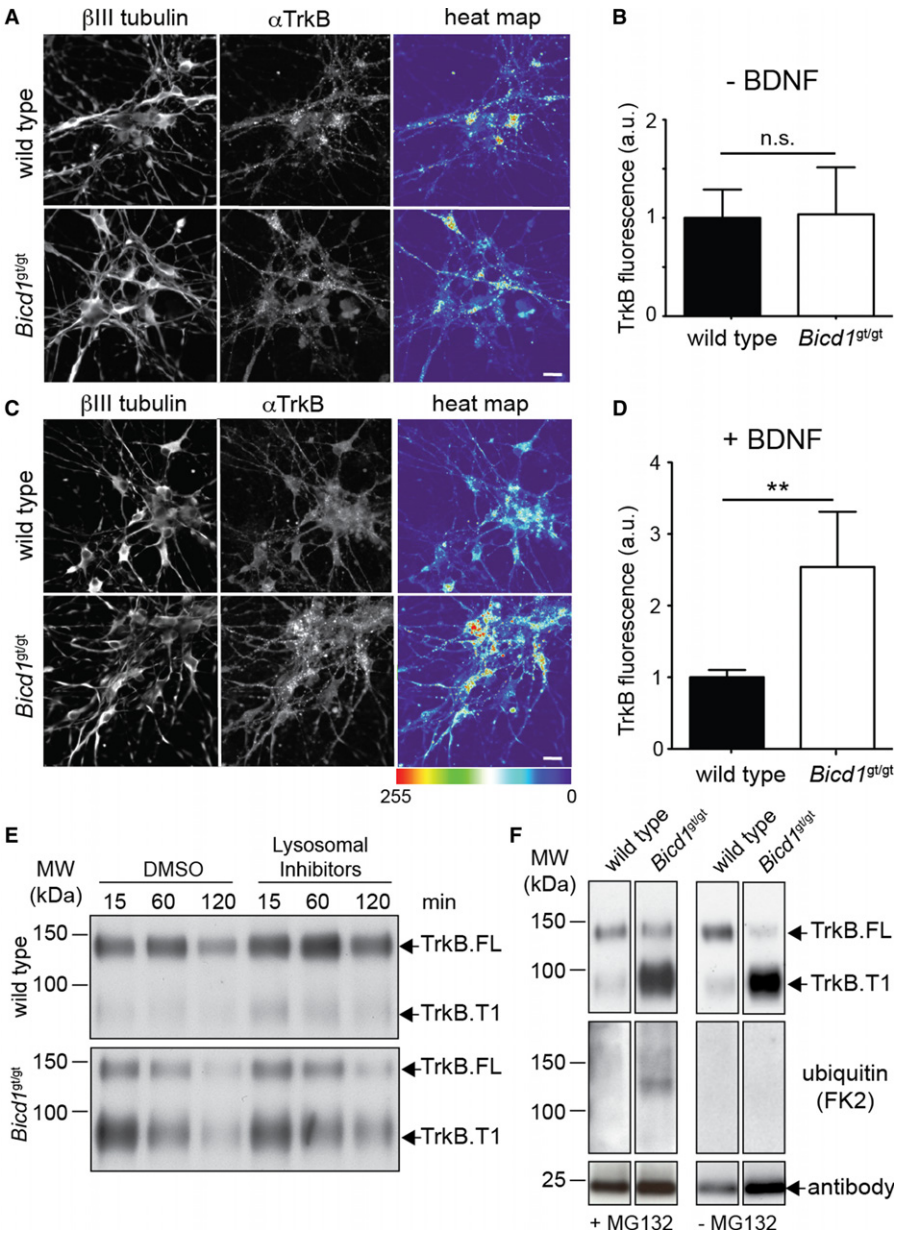

Figure 5. *Bicd1*$^{gt/gt}$ motor neurons (MNs) show increased brain-derived neurotrophic factor (BDNF)-dependent intracellular accumulation of TrkB, which is unaffected by treatment with lysosomal protease inhibitor.

A TrkB antibody (αTrkB) was internalised for 1 h at 37°C by wild-type and *Bicd1*$^{gt/gt}$ MNs, which were then acid-washed, fixed and immunostained for βIII tubulin and AlexaFluor-conjugated anti-rabbit IgG to detect αTrkB. Scale bar, 20 μm.

B Quantification of internalised αTrkB from three independent experiments (n = 3, t-test, mean ± s.e.m.; n.s., not significant).

C Internalisation of αTrkB as described for (A), but stimulated with 100 ng/ml of BDNF. Scale bar, 20 μm.

D Quantification of internalised αTrkB in the presence of BDNF from three independent experiments (n = 3, t-test, mean ± s.e.m., $^{**}P < 0.01$).

E Wild-type and *Bicd1*$^{gt/gt}$ MNs were co-incubated with αTrkB, 100 ng/ml of BDNF and a cocktail of lysosomal inhibitors (leupeptin 200 μM, E64D 2 μM, pepstatin A 20 μM) or DMSO vehicle control for 15 min at 37°C. Unbound antibody was then removed by repeated washing before chasing the internalised αTrkB pool under identical conditions.
Cells were subsequently lysed at different time points and αTrkB captured on protein-G-conjugated magnetic beads followed by western blotting for TrkB.
Note that the truncated TrkB.T1 isoform was significantly enriched relative to TrkB.FL in *Bicd1*$^{gt/gt}$ MNs (lower panel) compared to wild-type controls (upper panel).
Inhibition of lysosomal proteases prevented αTrkB.FL degradation in wild-type MNs (compare with DMSO-treated samples), but was ineffective in *Bicd1*$^{gt/gt}$ cells.

F Wild-type and *Bicd1*$^{gt/gt}$ MNs were co-incubated with αTrkB, 100 ng/ml of BDNF and lysosomal inhibitors as described in (E) for 15 min at 37°C in the presence or absence of 10 μM MG132. Upon cell lysis, αTrkB was captured as above. Immunoprecipitated samples were probed for TrkB (upper panels), with the FK2 antibody, which targets mono- and poly-ubiquitinated proteins (middle panels), and with horseradish peroxidase-conjugated anti-rabbit immunoglobulins in order to detect internalised αTrkB. TrkB.T1 was enriched in *Bicd1*$^{gt/gt}$ MNs in both conditions, but TrkB ubiquitination was detected only in *Bicd1*$^{gt/gt}$ MN samples treated with MG132.

Source data are available online for this figure.

TrkB and $p75^{NTR}$ in large vacuoles often connected to structures resembling tubular endosomes (Supplementary Fig S3D). Further insights into the nature of these organelles were provided by the co-localisation of SNX1 with TrkB and H_CT (Fig 3B and Supplementary Fig S4A and B), and the increase in SNX1-associated H_CT-positive structures in *Bicd1*$^{gt/gt}$ MNs (Supplementary Fig S4A and B). Based on these findings and the notion that TrkB was preferentially ubiquitinated when BICD1 was depleted (Fig 5F), we decided to test whether the altered neurotrophin receptor trafficking observed in *Bicd1*$^{gt/gt}$ MNs resulted in an increased recycling of these receptors back to the plasma membrane.

In spite of TrkB-FL transcript (Supplementary Fig S1D) and Trk protein levels (Fig 1E and F) being reduced in *Bicd1*$^{gt/gt}$ MNs relative to wild-type cells, cell surface immunofluorescence and biotinylation experiments both demonstrated that significantly more TrkB was present on the plasma membrane of *Bicd1*$^{gt/gt}$ neurons compared to wild-type controls (Fig 6A–E), with a similar trend also observed for $p75^{NTR}$ (Supplementary Fig S7A–D).

TrkB signalling is impaired in *Bicd1*$^{gt/gt}$ MNs

The most striking finding from the previous set of experiments was the substantial increase in TrkB.T1 localisation to the surface of *Bicd1*$^{gt/gt}$ MNs (Fig 6C–E). TrkB.T1 heterodimerises with TrkB.FL to inhibit auto-phosphorylation and downstream signalling of the full-length receptor (Eide *et al*, 1996; Fenner, 2012). Therefore, the substantially decreased ratio of TrkB.FL to TrkB.T1 (Fig 6E) on the plasma membrane of *Bicd1*$^{gt/gt}$ MNs, together with an increased cell surface localisation of $p75^{NTR}$ (Supplementary Fig S7A–D), would be expected to reduce phosphoinositide-3 kinase (PI3K) and Ras-mediated signal activation following treatment with BDNF.

To test this hypothesis, we stimulated MNs with BDNF for various time points before assaying lysates by western blotting for phosphorylated TrkB, AKT and ERK1/2. In wild-type cultures, both AKT and ERK1/2 phosphorylation peaked at 10 min followed by a progressive attenuation of this response over the following 40 min. The same overall trend was observed for *Bicd1*$^{gt/gt}$ MNs, but phosphorylation of both AKT and ERK1/2 was lower at all time points tested (Fig 7A–D). Thus, even though more cell surface TrkB and $p75^{NTR}$ were available for ligand binding in *Bicd1*$^{gt/gt}$ MNs, this was accompanied by decreased activation of AKT and ERK1/2 following BDNF treatment. This reduced signalling response might be a consequence of decreased TrkB activation caused by the lower TrkB.FL to TrkB.T1 ratio present in *Bicd1*$^{gt/gt}$ MNs. This hypothesis was supported by data shown in Fig 7E–F, where phosphorylation of TrkB upon stimulation with BDNF for 10 min was lower in mutant MNs compared to wild-type controls.

Proteosomal inhibition is known to induce sustained ERK1/2 activation following NGF stimulation (Moises *et al*, 2009), which was likely to result from enhanced TrkA recycling back to the plasma membrane. We now show that *Bicd1*$^{gt/gt}$ MNs respond to BDNF/TrkB activation through sustained PI3K/AKT signalling. Thus, whereas the phospho-AKT (pAKT) profile tailed off at later time points in wild-type cells, BICD1-depleted MNs displayed a more prolonged AKT activation during 1 h of BDNF stimulation (Fig 7A–B). This trend was substantiated by prolonged stimulation experiments when phospho-AKT levels, albeit lower, remained relatively stable over the entire time frame of the experiment in *Bicd1*$^{gt/gt}$ MNs (Fig 7G).

Discussion

Using a novel siRNA-screening approach designed to identify new players involved in the trafficking of neurotrophin receptors and neurotropic virulence factors in MNs (Terenzio *et al*, 2014), we identified several genes that affected the intracellular accumulation of H_CT and $\alpha p75^{NTR}$. Because of our long-standing interest in axonal retrograde transport, the most intriguing candidate revealed by this screen was *Bicd1*. This cytoplasmic dynein adaptor and closely related proteins, such as BICD2 and BICDR1, play diverse roles in nervous system development and maintenance (Matanis *et al*, 2002; Schlager *et al*, 2010). For instance, BICD2 is required for neuronal migration (Jaarsma *et al*, 2014), whereas BICD1 co-operates with dynein and kinesins in *C. elegans* nervous system patterning (Aguirre-Chen *et al*, 2011). Furthermore, *Drosophila* BicD recycles clathrin heavy chain back to the plasma membrane during synaptic stimulation (Li *et al*, 2010) and controls distribution of Fragile X mental retardation protein (Bianco *et al*, 2010). Our *in vivo* observations now expand this list of functions by showing that BICD1 very likely plays an important role in the developing mouse nervous system, at least during the period when BDNF and neurotrophin receptors are highly expressed (Fig 1 and Supplementary Fig S1).

Silencing of *Bicd1* increased the intracellular accumulation of H_CT, and this was confirmed in MNs expressing the RRP227 *Bicd1*$^{gt/gt}$ hypomorphic allele. The intracellular distribution of H_CT in *Bicd1*$^{gt/gt}$ MNs differed markedly from that observed in wild-type cells (Fig 2D and E). In mutant cells, H_CT clustered near the limiting membrane of a population of enlarged organelles with amorphous content, which lacked intra-luminal vesicles typical of MVBs (Fig 2D) and was found in protrusions emanating from such structures (Supplementary Fig S3D). These observations suggested that endosomal sorting and/or maturation of these H_CT-containing compartments were perturbed in *Bicd1*$^{gt/gt}$ MNs. Because H_CT is co-transported with $p75^{NTR}$ and TrkB, we inferred that these receptors were also likely to be present in at least a sub-population of the enlarged H_CT-labelled compartments present in *Bicd1*$^{gt/gt}$ MNs. This notion was supported by the findings that colloidal gold-labelled H_CT, αTrkB and $\alpha p75^{NTR}$ all accumulated in the same enlarged organelles (Fig 4), which strongly suggested that these structures represented sorting compartments common to all three probes. Furthermore, the increased occurrence of such organelles in *Bicd1*$^{gt/gt}$ MNs indicated that BICD1 depletion affected the endosomal sorting of H_CT, TrkB and $p75^{NTR}$.

This hypothesis was supported by the observation that H_CT-positive organelles in *Bicd1*$^{gt/gt}$ MNs also displayed an increased co-localisation with SNX1, a retromer component (Supplementary Fig S4A and B; Terenzio *et al*, 2014). Retromer is a large protein complex, which controls the endosome membrane re-sculpturing process essential for the formation of transport carriers (Bonifacino & Hurley, 2008; Cullen & Korswagen, 2012) and the selection of specific cargoes (Harrison *et al*, 2014). Classically, this complex has been shown to mediate retrograde transport of membrane-bound cargoes from endosomes to the trans-Golgi network (TGN).

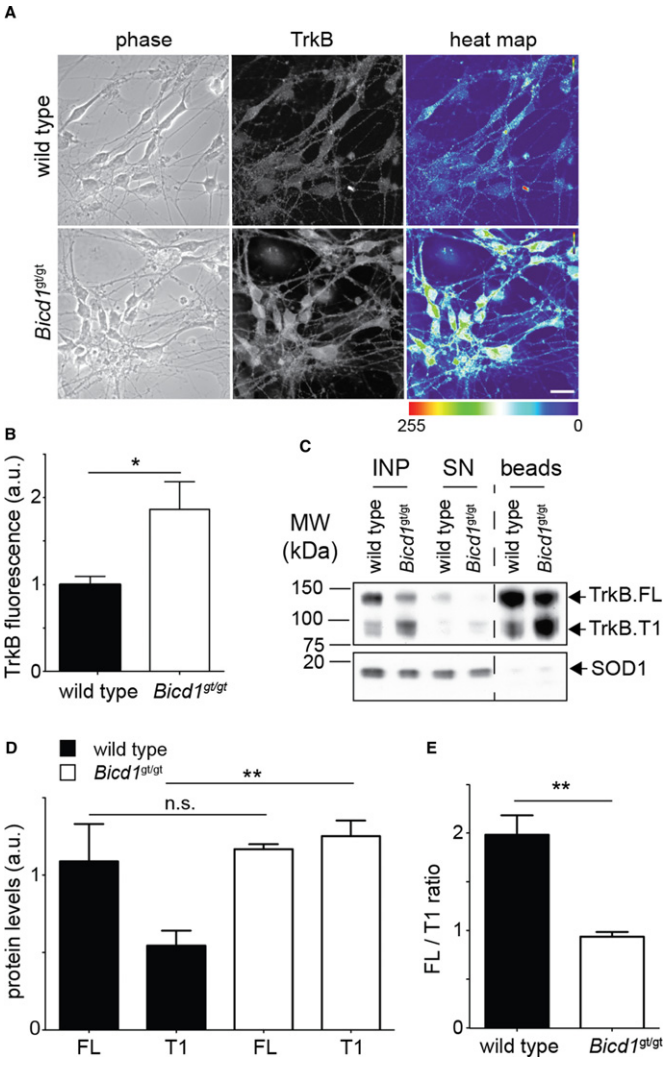

Figure 6. *Bicd1*$^{gt/gt}$ motor neurons (MNs) have increased cell surface levels of TrkB.T1.

A Wild-type and *Bicd1*$^{gt/gt}$ MNs were fixed and immunostained without permeabilisation to detect cell-surface-exposed TrkB using the TrkB antibody used in Fig 5. Scale bar, 20 μm.

B Quantification of cell-surface-localised TrkB receptors from three independent experiments (n = 3, t-test, mean ± s.e.m., *P < 0.05).

C Representative western blotting of TrkB isoforms present on the surface of wild-type and *Bicd1*$^{gt/gt}$ MNs at steady state. Cell surface proteins were biotinylated, purified on neutravidin sepharose beads and probed for the extracellular domain of TrkB. SOD1 was used as a control for cytosolic proteins. The input (INP), supernatant (SN) and biotinylated cell surface protein (beads) fractions are shown. Note the significantly increased level of TrkB.T1 relative to TrkB.FL in *Bicd1*$^{gt/gt}$ MNs compared to wild-type controls.

D Quantification of cell-surface-biotinylated TrkB.FL and TrkB.T1 receptors in (C) (t-test; mean ± s.e.m.; **P < 0.001, n.s., not significant, n = 4).

E TrkB.FL/TrkB.T1 receptor ratio (t-test; mean ± s.e.m.; **P < 0.001, n = 4).

Source data are available online for this figure.

However, Steinberg *et al* have recently shown that the retromer and specific SNX isoforms, such as SNX17 and SNX27, were involved in preventing lysosomal degradation in favour of maintaining plasma membrane levels of several transporters, signalling receptors and adaptor molecules, such as the glucose transporter GLUT1, PDGFRβ and the neurotrophin receptor-binding protein Kidins220/ARMS (Steinberg *et al*, 2012, 2013). Moreover, retromer-independent functions for SNX1 in the recycling of specific receptors to the plasma membrane have also been described (Nisar *et al*, 2010). The retrograde pathway to the TGN is unlikely to be involved in the re-routing of H_CT and neurotrophin receptors when BICD1 is depleted, since cholera toxin B subunit (CTB) trafficking to the Golgi was unaffected in *Bicd1*$^{gt/gt}$ MNs (Supplementary Fig S8). Importantly, this result also demonstrated that the depletion of BICD1 did not cause a general defect in endosomal trafficking.

Similar increased accumulation phenotypes in *Bicd1*$^{gt/gt}$ MNs were also observed for p75^{NTR} and TrkB, but only after treatment with BDNF (Fig 5A–D and Supplementary Fig S5A–D). Upon stimulation, phosphorylated TrkB is mainly sorted to lysosomes and degraded (Chen *et al*, 2005; Bronfman *et al*, 2007; Huang *et al*, 2009). Our observations that the intracellular accumulation of p75^{NTR} and TrkB was enhanced in *Bicd1*$^{gt/gt}$ MNs and that H_CT appeared to be trapped in organelles resembling those shown to accumulate NGF in sympathetic neurons treated with lysosomal inhibitors (Claude *et al*, 1982) suggested that the trafficking of receptors normally targeted to lysosomes might be impaired by BICD1 depletion. Accordingly, inhibiting lysosomal proteases in wild-type MNs phenocopied the increased accumulation of TrkB and p75^{NTR} observed in *Bicd1*$^{gt/gt}$ cultures treated with BDNF (Supplementary Fig S6A and B). These data, together with the lack of overt alterations in lysosome morphology or activity in *Bicd1*$^{gt/gt}$ MNs, implied that BICD1 is not likely to be involved in lysosome biogenesis or function, but participates in a sorting step regulating the targeting of endocytic cargoes to this organelle (Fig 8). TrkB antibody feeding assays confirmed this view by demonstrating that upon treatment with BDNF, TrkB internalised by *Bicd1*$^{gt/gt}$ MNs was not protected from degradation in the presence of lysosome protease inhibitors (Fig 5E). This result suggested that TrkB-BDNF complexes were preferentially degraded by an alternative mechanism in these cells. This was likely to be via the proteasome since ubiquitinated TrkB was detected only in immunoprecipitates retrieved from *Bicd1*$^{gt/gt}$ MNs in which proteasomal activity was inhibited (Fig 5F). Trk receptors have been shown to be ubiquitinated, and a proportion of this modified receptor pool is degraded by the proteasome (Sommerfeld *et al*, 2000; Geetha & Wooten, 2008). This post-translational modification is important for neurotrophin receptor function since defective ubiquitination of TrkA causes defective endosomal trafficking, impaired degradation and increased recycling of this receptor, which was proposed to lead to the increased survival of sensory neurons *in vivo* (Yu *et al*, 2014). Our findings now suggest that BICD1 plays a role in this pathway by regulating the balance between these two degradation fates. We speculate that impaired targeting of TrkB to lysosomes in neurons lacking BICD1 might cause an increased ubiquitination and re-routing of this receptor to the proteasome and the recycling pathway, resulting in the increased targeting of TrkB and p75^{NTR} to the plasma membrane, possibly via a SNX/retromer-mediated retrieval route (Fig 8). Such a mechanism would be expected to ensure appropriate TrkB-mediated signalling output in response to BDNF availability and according to the composition of receptor complexes bound to this ligand.

Several lines of evidence indicate that impairments of the trafficking and/or degradation of neurotrophin receptors alter the

output of neurotrophin-signalling cascades (Reichardt, 2006; Ascano *et al*, 2012). For example, overexpression of Hrs, a component of the endosomal sorting complex required for transport (ESCRT), in PC12 cells, caused a redirection of TrkB to the recycling route and a more sustained ERK1/2 activation upon BDNF treatment (Huang *et al*, 2009). Similar behaviour has also been described for TrkA in the same cell line, where inhibition of endosomal maturation by overexpression of a dominant-negative Rab7 mutant resulted in the accumulation of TrkA-containing endosomes and an increased ERK1/2 signalling (Saxena *et al*, 2005). Furthermore, proteosomal inhibition induced a sustained NGF-dependent ERK1/2 activation (Moises *et al*, 2009). Based on these results, we investigated the signalling responses to BDNF in *Bicd1*$^{gt/gt}$ MNs and found that TrkB phosphorylation and the downstream activation of PI3K-AKT and Ras-ERK1/2 were decreased in *Bicd1*$^{gt/gt}$ MNs (Fig 7). Notably, AKT phosphorylation levels, albeit lower, remain stable over a longer period in *Bicd1*$^{gt/gt}$ MNs compared to wild-type cells (Fig 7G), supporting the notion that receptor recycling is an important mechanism to sustain signalling by rapidly returning growth factor receptors to the plasma membrane (Chen *et al*, 2005; Huang *et al*, 2013).

A likely explanation for the lower signalling capacity of *Bicd1*$^{gt/gt}$ MNs is the reduced quantity of signalling-competent TrkB.FL relative to the dominant inhibitory TrkB.T1 isoform present on the surface of BICD1-depleted neurons (Fig 6C–E). This change in the stoichiometry of TrkB pools combined with the increased levels of p75^{NTR} on the cell surface of *Bicd1*$^{gt/gt}$ MNs may represent an adaptive response to overstimulation caused by defective degradation of activated TrkB.FL. In this light, BICD1-depleted MNs could adapt to these unfavourable conditions by altering their cell surface levels of p75^{NTR} and repertoire of TrkB isoforms in order to protect themselves from chronic TrkB.FL-mediated overstimulation, which is in agreement with the neuronal response to excitotoxic insult during brain ischaemia and traumatic brain injury (Gomes *et al*, 2012).

In conclusion, we would like to propose a model by which BICD1 controls the trafficking of activated neurotrophin receptors to appropriate degradation routes in order to maintain an optimal response to neurotrophin stimulation. By impinging on this trophic response, BICD1 functions to modulate both the signalling amplitude and duration elicited by ligand-bound neurotrophin receptors. In this context, BICD1 serves to fine-tune neurotrophin receptor signalling by maintaining the balance between receptor degradation over recycling so that the receptor pool not destined for degradation is targeted back to the plasma membrane by a retromer-mediated sorting process (Fig 8). This equilibrium ensures optimal signal intensity and/or duration by delivering the appropriate repertoire of neurotrophin receptors to the plasma membrane where they are available to respond to their cognate ligands, which are especially abundant during neuronal growth. BICD1 function would therefore be expected to be critical during nervous system development when neurons rely on neurotrophins for their specification, differentiation and survival. Indeed, this may be one reason why BICD1 is highly expressed together with neurotrophins and their receptors in the developing nervous system (Fig 1 and Supplementary Fig S1). TrkB-BDNF-signalling mechanisms are instrumental in regulating nervous system development and are key modulators of synaptic plasticity in adulthood. Intriguingly, dendritic elongation and branching of cortical neurons is controlled by the differential activation of TrkB.FL versus TrkB.T1 (Yacoubian & Lo, 2000), whilst p75^{NTR} is a negative modulator of dendrite complexity in hippocampal neurons (Zagrebelsky *et al*, 2005). These functions are very likely to operate in concert with BICD1, which was recently shown to be essential for the correct neuronal patterning and dendritic branching in *C. elegans* (Aguirre-Chen *et al*, 2011). These studies and our current work collectively indicate that BICD1 helps to coordinate the complex membrane sorting of neurotrophin-signalling endosomes during nervous system development and may regulate the activity of other receptor tyrosine kinases in different cell types.

Materials and Methods

Ethics statement

All experiments were carried out following the guidelines of the Cancer Research UK genetic manipulation procedures. Animal work was carried out under licence from the UK Home Office in accordance with the Animals (Scientific Procedures) Act 1986.

Reagents

Unless stated otherwise, all chemical reagents were supplied by Sigma. Tissue culture media, supplements and AlexaFluor555-conjugated CTB and secondary antibodies were purchased from Life Technologies.

Antibodies

Actin (AC-15), BICD1 (HPA041309), BICD2 (HPA024452) and FLAG (M1) were all obtained from Sigma. BDNF (N-20), LAMP2 (ABL-93), Rab6 and pan-Trk (C-14) were purchased from Santa Cruz. AKT (#9272), phospho-AKT (S473, #4060), ERK1/2 (#9102), phospho-ERK1/2 (#9101), TrkB (80E3) and phospho-TrkB (Y706/707, C50F3) were obtained from Cell Signalling. TrkB antibody (#07-225, used for live cell internalisation assays) and MAP2 were purchased from Millipore; βIII tubulin (TUJ1) was obtained from Covance; HB9 and SOD1 (ab16831) were obtained from Abcam; Islet1/2 was purchased from Developmental Studies Hybridoma Bank; FK2 was obtained from Enzo Life Sciences; mouse monoclonals to p150^{Glued} and p50 were purchased from BD Biosciences. αp75^{NTR} (5410) was described in (Deinhardt *et al*, 2007). SNX1 and Vps26 antibodies were a kind gift of Matthew Seaman, University of Cambridge, UK.

BDNF-mCherry expression

A BDNF-mCherry expression construct was kindly provided by F. Saudou (Institut Curie, Orsay, F; Gauthier *et al*, 2004) and transfected using Lipofectamine 2000 (Life Technologies) into HEK293-FT cells, which had previously been adapted to grow in suspension in HyClone Serum-Free Medium (SFM; Thermo Scientific). SFM conditioned with secreted BDNF-mCherry was collected after 72 h, centrifuged at high speed and the supernatant concentrated

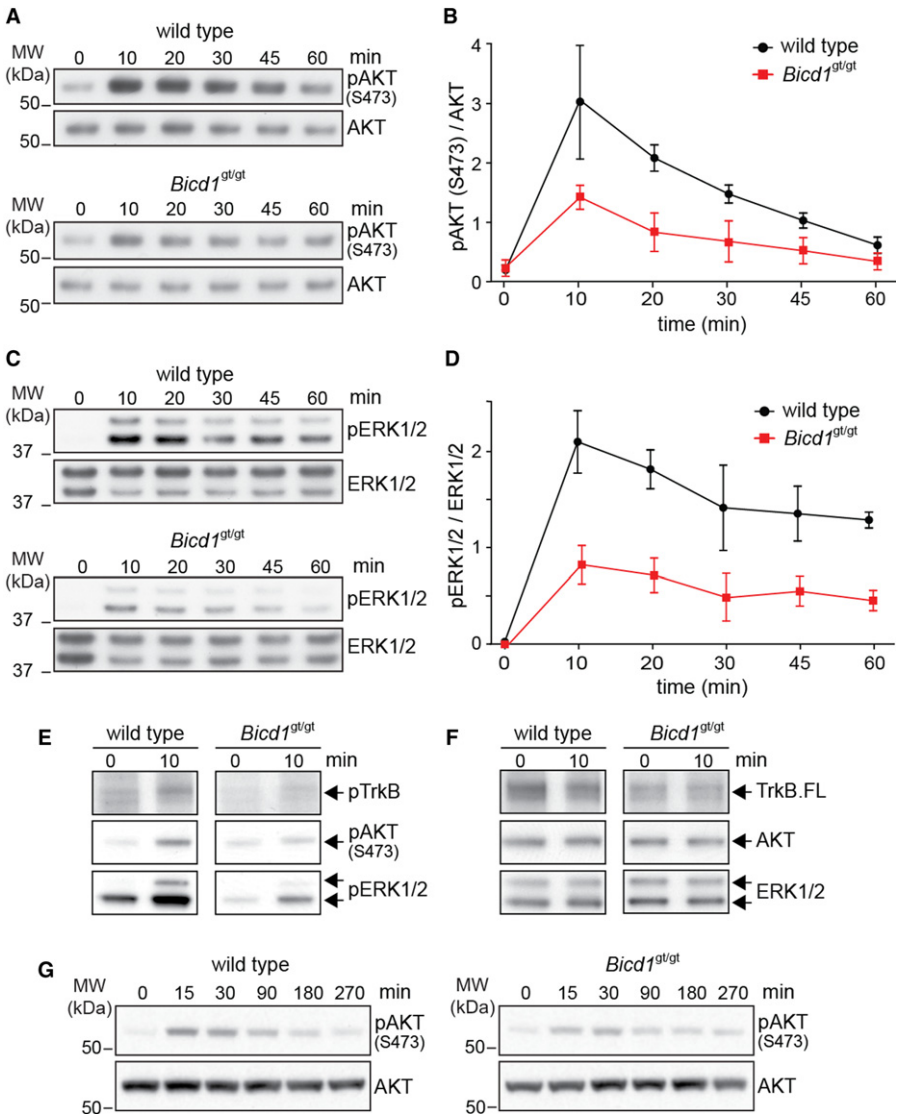

Figure 7. AKT and ERK1/2 phosphorylation are altered in brain-derived neurotrophic factor (BDNF)-stimulated *Bicd1*$^{gt/gt}$ motor neurons (MNs).

A Starved wild-type and *Bicd1*$^{gt/gt}$ MNs were stimulated with 100 ng/ml BDNF for various time points before cell lysis and immunoblotted for phospho-AKT (pAKT; S473) and then re-probed for total AKT.

B Densitometric analysis of pAKT (S473) from three independent experiments including the one shown in (A). pAKT band densities were normalised to total AKT (pAKT/AKT) for each time point and plotted as the mean ± s.e.m. Reduced phosphorylation of AKT in *Bicd1*$^{gt/gt}$ MNs compared to wild-type controls was statistically significant at all time points (two-way ANOVA, $P < 0.0001$).

C Starved wild-type and *Bicd1*$^{gt/gt}$ MNs were stimulated with 100 ng/ml BDNF for various time points before lysis and immunoblotted for phospho-ERK1/2 (pERK1/2) and then re-probed for total ERK1/2.

D Densitometric analysis of pERK1/2 from three independent experiments including the one shown in (C). pERK1/2 band densities were normalised to total extracellular signal-regulated kinase (ERK; pERK/ERK) for each time point and plotted as the mean ± s.e.m. Reduced phosphorylation of ERK1/2 in *Bicd1*$^{gt/gt}$ MNs compared to wild-type controls was statistically significant at all time points (two-way ANOVA, $P < 0.0001$).

E, F Starved wild-type and *Bicd1*$^{gt/gt}$ MNs were stimulated with 100 ng/ml BDNF for 10 min before cell lysis. Samples were immunoblotted for phospho-TrkB (pTrkB; top panel), phospho-AKT (pAKT; S473; middle panels) and pERK1/2 (lower panels) (E). The same lysates were probed for total TrkB, AKT and ERK1/2 to assess loading parity between samples (F).

G Starved wild-type (left panels) and *Bicd1*$^{gt/gt}$ MNs (right panels) were stimulated with 100 ng/ml BDNF for different times before cell lysis. Samples were immunoblotted for phospho-AKT (pAKT; S473) and total AKT. Note that there was a gradual decrease in pAKT signal over time for wild-type cells, which contrasted with sustained pAKT levels for *Bicd1*$^{gt/gt}$ MNs.

Source data are available online for this figure.

approximately 15-fold by force filtration using Amicon Ultra Centrifugal filters (Ultracel 30K; Millipore). The concentrate was snap frozen at −80°C and then analysed by western blotting against recombinant BDNF (R&D Systems) to assess BDNF-mCherry concentration (Deinhardt *et al*, 2006b) before performing FLAG-TrkB internalisation experiments in N2A cells.

Bicd1$^{gt/+}$ chimeric embryos and lacZ expression analysis

10–15 RRP227 ES cells were injected into blastocyst stage embryos collected from superovulated C57BL/6J female mice that had been mated to C57BL/6J male mice. Embryos were transferred to pseudo-pregnant (2.5 days post-coitum) recipient mice according to standard protocols (Nagy *et al*, 2003). To assess Bicd1-lacZ expression patterns during mouse development, E11.5-E14.5 embryos were fixed at room temperature for 15–30 min in 0.1 M sodium phosphate, pH 7.3, 0.4% paraformaldehyde (PFA), 5 mM EGTA, 2 mM $MgCl_2$, washed three times in 0.1 M sodium phosphate pH 7.3, 2 mM $MgCl_2$, 0.1% sodium deoxycholate, 0.02% NP-40 and finally transferred into developing solution (100 mM sodium phosphate, pH 7.3, 2 mM $MgCl_2$, 0.01% sodium deoxycholate, 0.02% NP-40, 5 mM $K_3Fe(CN)_6$, 5 mM $K_4Fe(CN)_6$, 1 mg/ml X-gal (Roche), for 30 min to 5 h at 37°C or overnight in the dark. The reaction was quenched by rinsing several times in PBS, and embryos were then post-fixed in 4% PFA and stored in 70% ethanol prior to imaging. After imaging, some samples were paraffin embedded, sectioned, DAB immunostained and counterstained with Nile red.

Embryonic stem-cell-derived MNs

Embryonic stem cells were grown on fish skin gelatin-coated flasks in Glasgow Minimal Essential Medium (GMEM), 5% ES cell-qualified foetal bovine serum FBS, 5% knockout serum replacement (KSR), 1% GLUTAMAX, 0.1 mM 2-mercaptoethanol and 1,000 units/ml of leukaemia inhibitory factor (ESGRO, Millipore). To generate MNs, 1.5×10^6 ES cells were grown in suspension on a 10-cm non-tissue culture-treated Petri dish containing differentiation (DFNK) medium: 45% neurobasal, 45% DMEM/Ham's-F12, 10% KSR, 1% GLUTAMAX and 0.1 mM 2-mercaptoethanol. The following day, embryoid bodies (EBs) were gently centrifuged and re-suspended in 10 ml of fresh DFNK medium and plated on a new Petri dish. The following day, the greatly enlarged EBs were allowed to sediment by gravity and re-suspended in fresh DFNK medium supplemented with 1 μM all-trans retinoic acid (RA) and 333 nM Smoothened Agonist (SAG; Enzo Life Sciences). EBs were maintained under these conditions for a further 4 days (medium changed every other day) and then dissociated with 0.025% porcine pancreatic trypsin in 1 ml PBS for 7 min at 37°C and processed as described previously for the dissociation of mouse E13.5 spinal cord MNs (Hafezparast *et al*, 2003). Cells were plated onto poly-D-ornithine and laminin-coated dishes in MN growth medium: neurobasal medium supplemented with 2% B27, 2% heat-inactivated horse serum, 1% GLUTAMAX, 25 μM 2-mercaptoethanol, 10 ng/ml rat ciliary neurotrophic factor (CNTF; R&D Systems), 100 pg/ml rat glial cell line-derived neurotrophic factor (GDNF; R&D Systems) and 1 μM RA.

Generation of homozygous RRP227 ES cells

Mouse ES cells with a gene trap insertion in the first intron of *Bicd1* (RRP227; http://www.informatics.jax.org/allele/key/544886) were obtained from the Mutant Mouse Regional Resource Center. Homozygous *Bicd1*$^{gt/gt}$ cells were generated as previously described (Lefebvre *et al*, 2001). Briefly, heterozygous cells were seeded at 30% confluence and maintained under standard feeder-free ES cell culture

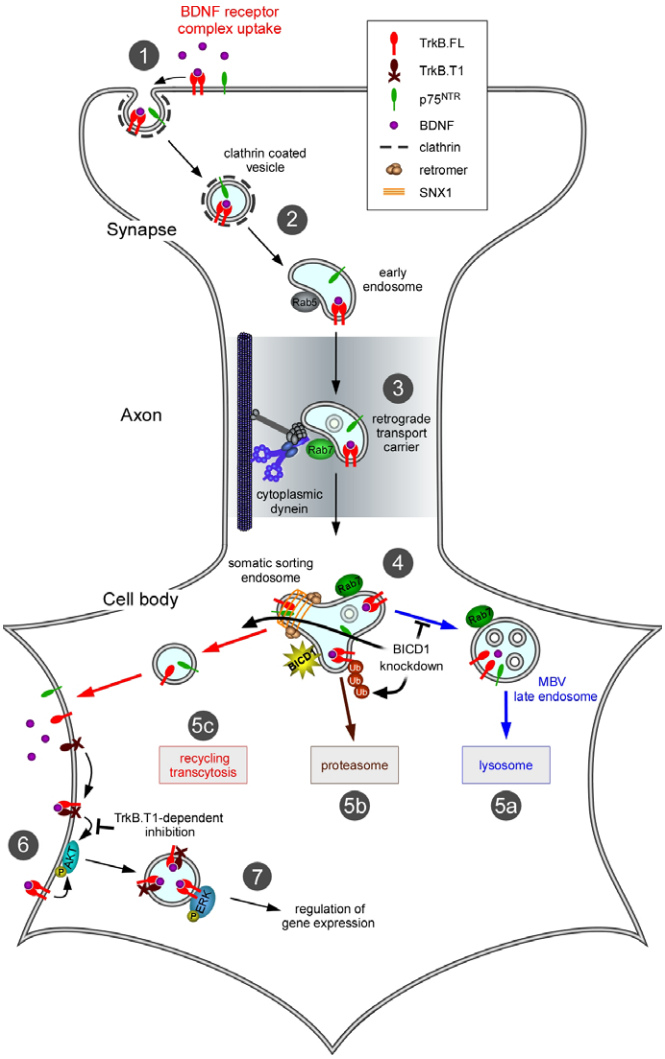

Figure 8. Proposed role of BICD1 in neurotrophin receptor trafficking and signalling.
In wild-type motor neurons (MNs), brain-derived neurotrophic factor (BDNF) binds to and activates TrkB. Ligand–receptor complexes are internalised at synaptic sites located in the periphery (1); note that for clarity, internalisation of these complexes from the plasma membrane of the cell body is not depicted. Ligand–receptor complexes are sorted to signalling endosomes (2), retrogradely transported in a cytoplasmic dynein-dependent process (3), towards the cell soma where they associate with somatic sorting endosomes (4) decorated by sorting nexin 1 (SNX1) and other retromer components. Different neurotrophin receptor pools are then trafficked towards MVB/lysosomes (5a) or the proteasome (5b) for degradation, or recycled back to the plasma membrane (5c). Impairment of the lysosomal targeting of TrkB in cells lacking BICD1 is envisaged to impair the flow of the receptor from somatic sorting endosomes towards lysosomes and redirect them either to the recycling route back to the plasma membrane or to the proteasome for ubiquitin-mediated degradation. The main consequence of these mis-sorting steps is the increased accumulation of neurotrophin receptors on the cell surface at steady state. Such a chronic imbalance in receptor recycling over receptor degradation in *Bicd1*$^{gt/gt}$ MNs is predicted to result in prolonged receptor activation after internalisation and/or overstimulation from repeated recycling to the plasma membrane. The increased levels of cell surface TrkB.T1 in *Bicd1*$^{gt/gt}$ MNs (6) may be an adaptive response to overstimulation and serves to reduce BDNF-mediated activation of TrkB.FL and associated AKT (6) and ERK1/2 (7) signalling pathways.

conditions in medium containing 1.5 mg/ml G418 until distinct clones of antibiotic-resistant cells appeared. Several clones were picked up into a drop of 0.025% trypsin solution and seeded into separate wells of a 24-well plate and grown in the presence of 500 ng/ml G418. Loss of heterozygosity was assessed by semi-quantitative real-time PCR using the One-Step RT-PCR kit (Life Technologies) and primers specific for the wild-type *Bicd1* cDNA (forward: ggc tgg tgg tgc tgg agg aga a; reverse: gtg gac act agt ttc tgc aat gtg a).

The G418-resistant ES cell clone that showed the most marked reduction in PCR product relative to the heterozygous parent cell line was then selected for further quantification by quantitative real-time PCR, which confirmed an approximately 70% reduction in *Bicd1* expression relative to wild-type ES cells.

Quantitative real-time PCR

Total RNA was extracted from ES cell-derived MN cultures 4–5 days after the plating of disaggregated EBs, using either Trizol (Life Technologies) or RNeasy kits (Qiagen). One to 2 μg of total RNA was used to synthesise cDNA using the Superscript-VILO cDNA synthesis kit (Life Technologies). cDNA was diluted tenfold, and PCR amplified on a 7500 Fast Real-Time PCR (Applied Biosystems) using intron spanning primers (Supplementary Table S2) and EXPRESS SYBR Green ER master mix (Life Technologies).

BICD1-GFP and FLAG-TrkB overexpression in N2A cells

N2A cells were transfected with FLAG-TrkB constructs (kindly provided by Francis Lee, Weill Cornell Medical College, NY, USA) and BICD1-GFP using Lipofectamine 2000 according to the manufacturer's instructions. Approximately 13 h after transfection, antibody uptake experiments were performed on N2A cells by incubation with FLAG-tag antibody (clone M1, 1:1,000) in the presence either of recombinant BDNF (100 ng/ml) or purified mCherry-BDNF for 1 h at 37°C. Cells were then acid-washed for 2 min, washed in PBS and fixed with 4% PFA for 20 min. Cells were then immunostained with AlexaFluor555- or AlexaFluor488-conjugated anti-mouse antibodies to detect internalised FLAG-TrkB and primary antibodies targeting endogenous SNX1 or BICD1.

Immunofluorescence and immunohistochemistry

Motor neurons were seeded onto poly-D-ornithine and laminin-coated coverslips, maintained under standard culture conditions for 4–5 days before fixation with 4% PFA for 15 min at room temperature. Fixed cells were washed and blocked in 2% bovine serum albumin (BSA) in PBS with or without 0.2% Triton X-100 for 20 min at room temperature prior to incubation for 1 h with primary antibodies (see above) followed by AlexaFluor-conjugated secondary antibodies (1:500). Samples were then counterstained with DRAQ5 (Biostatus), post-fixed with PFA and mounted with Mowiol.

E11.5–14.5 embryos were fixed in neutral-buffered formalin overnight, processed for paraffin embedding and then sectioned. Sections (4 μm) were microwaved for 15 min in 0.01 M sodium citrate buffer, pH 6.0 for antigen retrieval, blocked with 10% normal donkey serum, 1% BSA and stained overnight at 4°C with a combination of mouse anti-βIII tubulin and either rabbit anti-BDNF (N-20), rabbit anti-pan-Trk (C-14) or $\alpha p75^{NTR}$ (5410). Following extensive washing in PBS, sections were stained with biotinylated horse anti-rabbit IgG (Vector Labs) and AlexaFluor488-conjugated donkey anti-mouse IgG for 1 h. After washing, sections were incubated in AlexaFluor555-conjugated streptavidin (Life Technologies) for 45 min at room temperature, washed, incubated for 30 min in 0.1% Sudan Black dissolved in 70% ethanol to quench auto-fluorescence and then mounted in Hardset Mount containing DAPI (Vector). The same protocol was used for horseradish peroxidase (HRP) immunohistochemistry except that sections were firstly quenched with 1.6% H_2O_2/PBS before blocking and staining with a single primary antibody, followed by biotinylated secondary antibody and ABC reagent (Vector Labs), developed with DAB (Vector Labs) and counterstained with haematoxylin.

Cell surface biotinylation

The pool of neurotrophin receptors on the plasma membrane was retrieved using a cell surface biotinylation kit (Thermo Scientific) according to the manufacturer's instructions. Briefly, wild-type and $Bicd1^{gt/gt}$ MNs were assayed under steady-state conditions 4–5 days after plating at high density onto 6-cm dishes, by cooling on wet ice before removing the growth medium, washing with ice-cold PBS and crosslinking cell-surface-exposed proteins with sulfo-NHS-SS-biotin for 30 min on ice. After quenching, cells were scraped, pelleted, washed twice with ice-cold Tris-buffered saline (TBS) and lysed on ice for 30 min. Insoluble proteins were pelleted by centrifugation and supernatants adjusted to the same protein concentration. Biotinylated proteins from 100 μg of total lysate were isolated with neutravidin agarose beads prior to western blot analysis.

Endosome isolation and Western blotting

MION-conjugated H_CT was used to purify H_CT-positive endosomes, which were isolated as previously described (Wade *et al*, 2012). SDS-PAGE was performed using 4–12% NuPAGE Bis-Tris gradient gels (Life Technologies) according to the manufacturer's instructions and blotted onto polyvinylidene fluoride (PVDF) membranes. Membranes were blocked in 5% skimmed milk or 5% BSA dissolved in TBS containing 0.05% Tween-20 (TBST) for 1 h at room temperature and then incubated with primary antibodies diluted 1:1,000 or 1:2,000 in TBST for 1 h at room temperature or overnight at 4°C. Blots were then washed and incubated with appropriate HRP-conjugated secondary antibodies (GE Healthcare). Immunoreactivity was detected using Luminata or Crescendo ECL substrates (Millipore) and ECL-Hyperfilm (GE Healthcare).

Internalisation assays

Internalisation assays for H_CT, $\alpha p75^{NTR}$ and αTrkB (Upstate, 1:1,000) were performed on wild-type and $Bicd1^{gt/gt}$ motor neurons seeded onto coverslips. Experiments designed to rescue the *Bicd1* depletion phenotypes were carried out on $Bicd1^{gt/gt}$ motor neurons transfected with a full length mouse *Bicd1* cDNA (MGC-27566, LGC Promochem) cloned into EcoR1/BamH1 sites of EGFP-N1 (Clontech).

This BICD1-GFP construct (see Terenzio et al., 2014) was transfected into motor neurons by Magnetofection using Neuromag (OZ Biosciences) following manufacturer's specifications. Cells were assayed within 16 h of transfection.

Pharmacological experiments

H_CT and $\alpha p75^{NTR}$ and αTrkB internalisation/accumulation assays were performed as described in the main text, but in the presence of lysosomal inhibitors (leupeptin 200 μM, E64D 2 μM, pepstatin A 20 μM) or an equivalent volume of DMSO. Cells were allowed to internalise the probes for 1 h at 37°C, acid-washed for 2 min, washed in PBS and fixed with 4% PFA for 20 min. To detect internalised $\alpha p75^{NTR}$ or αTrkB, the cells were immunostained with anti-rabbit AlexaFluor555-conjugated IgG.

For biochemical assessments of internalised receptor fate, a pulse-chase antibody feeding assay was performed as follows: MN cultures were incubated with αTrkB and BDNF in the presence or absence of lysosomal inhibitors in complete growth medium as described above, but instead of a 1-h continuous feed, a 15-min internalisation pulse was performed. This was followed by washing the cells three times with fresh antibody-free medium and incubation for a further 1 or 2 h as above, but in the absence of αTrkB. To assess TrkB ubiquitination, the same protocol was used with the addition of MG132 (10 μM), which was present throughout the pulse and chase periods. The quantity of initially internalised αTrkB/TrkB complex (15 min pulse) and non-degraded αTrkB/TrkB remaining after the chase periods was determined by immunoprecipitating the antibody/receptor complex from cell lysates prepared as described below for the signalling assays. Lysates were then incubated for 1 h at 4°C with 10 μl of pre-washed protein-G coated Dynabeads (Life Technologies) per sample. TrkB-bound beads were then washed three times in lysis buffer and captured antibodies eluted with Laemmlli sample buffer followed by SDS-PAGE and western blotting. The top half of these blots was first probed using the rabbit anti-TrkB (80E3) antibody. Some blots were then stripped and re-probed for ubiquitin using the mouse FK2 antibody. The lower half of these same blots were probed separately with HRP-conjugated anti-rabbit immunoglobulins in order to detect the immunoglobulin chains of internalised αTrkB.

Cholera toxin B subunit accumulation assay

Wild-type and $Bicd1^{gt/gt}$ MNs were allowed to internalise AlexaFluor555-CTB (1 μg/ml) for 1 h at 37°C, acid-washed for 2 min, washed in PBS and fixed with 4% PFA for 20 min. Samples were immunostained for βIII tubulin and imaged. The amount of CTB accumulation in the Golgi area was quantified using ImageJ.

Neurite outgrowth assay

Wild-type and $Bicd1^{gt/gt}$ MNs were plated at equal density, fixed 48 h after plating with 4% PFA for 20 min, immunostained for βIII tubulin and imaged. Quantification of total outgrowth, maximum process length and number of branches was performed using Metamorph (Molecular Devices).

Signalling assays

Wild-type and $Bicd1^{gt/gt}$ MNs were starved for 5 h at 37°C in neurobasal medium and then stimulated with 100 ng/ml of BDNF in the same medium. At the appropriate time points, cells were placed on ice immediately after removing the growth medium and then lysed in 10 mM Tris-HCl pH 8.0, 150 mM NaCl, 1% NP-40, 1 mM EDTA containing HALT protease and phosphatase inhibitors (Thermo Scientific) for 30 min. Insoluble proteins were pelleted and protein concentration assayed in the supernatants before addition of sample buffer. Samples were heated for 10 min at 70°C and 5–15 μg of protein per sample loaded in SDS-PAGE prior to western blotting for pTrkB, phospho-AKT and pERK1/2. Phosphorylation levels were quantified either by re-probing the same membranes, or in some cases, by running the same lysates in parallel and immunoblotting for the respective total proteins.

Axonal retrograde transport assay

Axonal retrograde transport kinetics of H_CT and $\alpha p75^{NTR}$ in wild-type and in $Bicd1^{gt/gt}$ MNs was performed as previously described (Lalli & Schiavo, 2002; Deinhardt *et al*, 2006b) and quantified using Motion Analysis software (Kinetic Imaging; Bohnert & Schiavo, 2005; Deinhardt *et al*, 2006b).

Transmission electron microscopy

H_CT was conjugated to colloidal gold by mixing 250 μg of purified H_CT in 0.5 ml of 2 mM sodium tetraborate to 1 ml of colloidal gold particles (10 nm; British Biocell) previously adjusted to pH 6.0. $\alpha p75^{NTR}$ (#5411; 200 μg in 0.2 ml) and αTrkB (#07-225; 60 μg in 0.2 ml) were dialysed against 2 mM sodium tetraborate and incubated with 2 ml (5 nm) and 0.2 ml (20 nm), respectively, of colloidal gold previously adjusted to pH 9.0. Samples were stirred at room temperature for 10 min. BSA was added to a final concentration of 1%, and the mixture stirred for a further 10 min. The suspension was finally pelleted at 45,000 *g* for 45 min ($\alpha p75^{NTR}$), 30 min (H_CT) and 10 min (αTrkB), resuspended in the original volume of 20 mM Tris-NaOH pH 8.2, 150 mM NaCl, 1% BSA and stored at 4°C for a maximum of 2–3 weeks.

Motor neurons plated on coverslips were incubated with 20 nM nanogold-conjugated H_CT for 2 h at 37°C prior to washing. Cells were fixed in 2.5% glutaraldehyde, 4% PFA in Sorensen's phosphate buffer at room temperature for 20 min, post-fixed in osmium tetroxide, stained with tannic acid and dehydrated progressively up to 100% ethanol. Finally, coverslips were embedded in an Epon epoxy resin, sectioned (70–75 nm) and stained with lead citrate. Images were acquired using a Tecnai Spirit Biotwin (FEI) transmission electron microscope. Random grids were visually scanned for the presence of nanogold-containing organelles by two independent operators and classified as described in the main text.

Data quantification

ImageJ was used for the quantification of western blots and immunofluorescence staining in all experiments. ImageJ was used to threshold the fluorescence staining of interest and quantify the thresholded voxels. Immunostaining for neuronal-specific proteins, such as βIII

tubulin, was used as object masks to quantify both immunostaining intensity as well as fluorescent probe binding and internalisation.

Supplementary information for this article is available online: http://emboj.embopress.org

Acknowledgements

We thank Michael Parkinson and Ken Blight for help with electron microscopy sample preparation and analyses, Frederic Saudou for BDNF-mCherry expression vector, Francis Lee for the FLAG-TrkB construct, Matthew Seaman for anti-SNX1 and Vps26 antibodies and members of the Molecular Neuropathobiology Laboratory for constructive comments. This work was supported by Cancer Research UK, the Marie Curie Actions Human Resources and Mobility Training Network 'Endocyte' (MRTN-CT-2006-035528; to MT), the FP7-HEALTH-2007-B grant 'BrainCAV' (FP7-222992; to GS) and Weizmann-UK 'Making Connections' grant (to GS).

Author contributions

MT designed, optimised and performed the siRNA screen, validated the resulting hits and analysed and interpreted the data. MG performed embryo analysis, biotinylation assays, antibody capture and signalling experiments and interpreted the data. BS-D carried out immunohistochemistry and tissue analyses. IR generated embryos from *Bicd1*$^{gt/+}$ ES cells. MG, MT and KW contributed to the remaining work. GS designed the study, contributed to data analyses and interpretation. DI-H provided critical comments and contributed to revision of the text. MG, MT and GS wrote the manuscript and assembled the figures.

Conflict of interest

The authors declare that they have no conflict of interest.

References

Aguirre-Chen C, Bulow HE, Kaprielian Z (2011) *C. elegans* bicd-1, homolog of the Drosophila dynein accessory factor Bicaudal D, regulates the branching of PVD sensory neuron dendrites. *Development* 138: 507 – 518

Ascano M, Bodmer D, Kuruvilla R (2012) Endocytic trafficking of neurotrophins in neural development. *Trends Cell Biol* 22: 266 – 273

Bercsenyi K, Giribaldi F, Schiavo G (2013) The elusive compass of clostridial neurotoxins: deciding when and where to go? *Curr Top Microbiol Immunol* 364: 91 – 113

Bianco A, Dienstbier M, Salter HK, Gatto G, Bullock SL (2010) Bicaudal-D regulates fragile X mental retardation protein levels, motility, and function during neuronal morphogenesis. *Curr Biol* 20: 1487 – 1492

Bibel M, Barde YA (2000) Neurotrophins: key regulators of cell fate and cell shape in the vertebrate nervous system. *Genes Dev* 14: 2919 – 2937

Bohnert S, Schiavo G (2005) Tetanus toxin is transported in a novel neuronal compartment characterized by a specialized pH regulation. *J Biol Chem* 280: 42336 – 42344

Bonifacino JS, Hurley JH (2008) Retromer. *Curr Opin Cell Biol* 20: 427 – 436

Bronfman FC, Escudero CA, Weis J, Kruttgen A (2007) Endosomal transport of neurotrophins: roles in signaling and neurodegenerative diseases. *Dev Neurobiol* 67: 1183 – 1203

Chen ZY, Ieraci A, Tanowitz M, Lee FS (2005) A novel endocytic recycling signal distinguishes biological responses of Trk neurotrophin receptors. *Mol Biol Cell* 16: 5761 – 5772

Claude P, Hawrot E, Dunis DA, Campenot RB (1982) Binding, internalization, and retrograde transport of ^{125}I-nerve growth factor in cultured rat sympathetic neurons. *J Neurosci* 2: 431 – 442

Cullen PJ, Korswagen HC (2012) Sorting nexins provide diversity for retromer-dependent trafficking events. *Nat Cell Biol* 14: 29 – 37

Davies AM (1994) The role of neurotrophins in the developing nervous system. *J Neurobiol* 25: 1334 – 1348

Deinhardt K, Berninghausen O, Willison HJ, Hopkins CR, Schiavo G (2006a) Tetanus toxin is internalized by a sequential clathrin-dependent mechanism initiated within lipid microdomains and independent of epsin1. *J Cell Biol* 174: 459 – 471

Deinhardt K, Salinas S, Verastegui C, Watson R, Worth D, Hanrahan S, Bucci C, Schiavo G (2006b) Rab5 and Rab7 control endocytic sorting along the axonal retrograde transport pathway. *Neuron* 52: 293 – 305

Deinhardt K, Reversi A, Berninghausen O, Hopkins CR, Schiavo G (2007) Neurotrophins Redirect p75^{NTR} from a clathrin-independent to a clathrin-dependent endocytic pathway coupled to axonal transport. *Traffic* 8: 1736 – 1749

Eide FF, Vining ER, Eide BL, Zang K, Wang XY, Reichardt LF (1996) Naturally occurring truncated trkB receptors have dominant inhibitory effects on brain-derived neurotrophic factor signaling. *J Neurosci* 16: 3123 – 3129

Ernfors P (2001) Local and target-derived actions of neurotrophins during peripheral nervous system development. *Cell Mol Life Sci* 58: 1036 – 1044

Fenner BM (2012) Truncated TrkB: beyond a dominant negative receptor. *Cytokine Growth Factor Rev* 23: 15 – 24

Fuchs E, Short B, Barr FA (2005) Assay and properties of rab6 interaction with dynein-dynactin complexes. *Methods Enzymol* 403: 607 – 618

Gauthier LR, Charrin BC, Borrell-Pages M, Dompierre JP, Rangone H, Cordelieres FP, De Mey J, MacDonald ME, Lessmann V, Humbert S, Saudou F (2004) Huntingtin controls neurotrophic support and survival of neurons by enhancing BDNF vesicular transport along microtubules. *Cell* 118: 127 – 138

Geetha T, Wooten MW (2008) TrkA receptor endolysosomal degradation is both ubiquitin and proteasome dependent. *Traffic* 9: 1146 – 1156

Gomes JR, Costa JT, Melo CV, Felizzi F, Monteiro P, Pinto MJ, Inacio AR, Wieloch T, Almeida RD, Graos M, Duarte CB (2012) Excitotoxicity downregulates TrkB.FL signaling and upregulates the neuroprotective truncated TrkB receptors in cultured hippocampal and striatal neurons. *J Neurosci* 32: 4610 – 4622

Hafezparast M, Klocke R, Ruhrberg C, Marquardt A, Ahmad-Annuar A, Bowen S, Lalli G, Witherden AS, Hummerich H, Nicholson S, Morgan PJ, Oozageer R, Priestley JV, Averill S, King VR, Ball S, Peters J, Toda T, Yamamoto A, Hiraoka Y *et al* (2003) Mutations in dynein link motor neuron degeneration to defects in retrograde transport. *Science* 300: 808 – 812

Harrison MS, Hung CS, Liu TT, Christiano R, Walther TC, Burd CG (2014) A mechanism for retromer endosomal coat complex assembly with cargo. *Proc Natl Acad Sci USA* 111: 267 – 272

Hirokawa N, Niwa S, Tanaka Y (2010) Molecular motors in neurons: transport mechanisms and roles in brain function, development, and disease. *Neuron* 68: 610 – 638

Hoogenraad CC, Akhmanova A, Howell SA, Dortland BR, De Zeeuw CI, Willemsen R, Visser P, Grosveld F, Galjart N (2001) Mammalian Golgi-associated Bicaudal-D2 functions in the dynein-dynactin pathway by interacting with these complexes. *EMBO J* 20: 4041 – 4054

Huang EJ, Reichardt LF (2001) Neurotrophins: roles in neuronal development and function. *Annu Rev Neurosci* 24: 677 – 736

Huang SH, Wang J, Sui WH, Chen B, Zhang XY, Yan J, Geng Z, Chen ZY (2013) BDNF-dependent recycling facilitates TrkB translocation to postsynaptic density during LTP via a Rab11-dependent pathway. *J Neurosci* 33: 9214 – 9230

Huang SH, Zhao L, Sun ZP, Li XZ, Geng Z, Zhang KD, Chao MV, Chen ZY (2009) Essential role of Hrs in endocytic recycling of full-length TrkB receptor but not its isoform TrkB.T1. *J Biol Chem* 284: 15126 – 15136

Ibanez CF (2007) Message in a bottle: long-range retrograde signaling in the nervous system. *Trends Cell Biol* 17: 519 – 528

Jaarsma D, van den Berg R, Wulf PS, van Erp S, Keijzer N, Schlager MA, de Graaff E, De Zeeuw CI, Pasterkamp RJ, Akhmanova A, Hoogenraad CC (2014) A role for Bicaudal-D2 in radial cerebellar granule cell migration. *Nat Commun* 5: 3411

Klein R (1994) Role of neurotrophins in mouse neuronal development. *FASEB J* 8: 738 – 744

Lalli G, Schiavo G (2002) Analysis of retrograde transport in motor neurons reveals common endocytic carriers for tetanus toxin and neurotrophin receptor p75NTR. *J Cell Biol* 156: 233 – 239

Lefebvre L, Dionne N, Karaskova J, Squire JA, Nagy A (2001) Selection for transgene homozygosity in embryonic stem cells results in extensive loss of heterozygosity. *Nat Genet* 27: 257 – 258

Li X, Kuromi H, Briggs L, Green DB, Rocha JJ, Sweeney ST, Bullock SL (2010) Bicaudal-D binds clathrin heavy chain to promote its transport and augments synaptic vesicle recycling. *EMBO J* 29: 992 – 1006

Matanis T, Akhmanova A, Wulf P, Del Nery E, Weide T, Stepanova T, Galjart N, Grosveld F, Goud B, De Zeeuw CI, Barnekow A, Hoogenraad CC (2002) Bicaudal-D regulates COPI-independent Golgi-ER transport by recruiting the dynein-dynactin motor complex. *Nat Cell Biol* 4: 986 – 992

Moises T, Wuller S, Saxena S, Senderek J, Weis J, Kruttgen A (2009) Proteasomal inhibition alters the trafficking of the neurotrophin receptor TrkA. *Biochem Biophys Res Commun* 387: 360 – 364

Nagy A, Gertsensten M, Vintersten K, Behringer R (2003) *Manipulating the Mouse Embryo; A Laboratory manual*, 3rd edn. New York: Cold Spring Harbor Press

Nisar S, Kelly E, Cullen PJ, Mundell SJ (2010) Regulation of P2Y1 receptor traffic by sorting Nexin 1 is retromer independent. *Traffic* 11: 508 – 519

Parton RG, Ockleford CD, Critchley DR (1987) A study of the mechanism of internalisation of tetanus toxin by primary mouse spinal cord cultures. *J Neurochem* 49: 1057 – 1068

Reichardt LF (2006) Neurotrophin-regulated signalling pathways. *Philos Trans R Soc Lond B Biol Sci* 361: 1545 – 1564

Salinas S, Bilsland LG, Schiavo G (2008) Molecular landmarks along the axonal route: axonal transport in health and disease. *Curr Opin Cell Biol* 20: 445 – 453

Saxena S, Bucci C, Weis J, Kruttgen A (2005) The small GTPase Rab7 controls the endosomal trafficking and neuritogenic signaling of the nerve growth factor receptor TrkA. *J Neurosci* 25: 10930 – 10940

Schlager MA, Kapitein LC, Grigoriev I, Burzynski GM, Wulf PS, Keijzer N, de Graaff E, Fukuda M, Shepherd IT, Akhmanova A, Hoogenraad CC (2010) Pericentrosomal targeting of Rab6 secretory vesicles by Bicaudal-D-related protein 1 (BICDR-1) regulates neuritogenesis. *EMBO J* 29: 1637 – 1651

Schmieg N, Menendez G, Schiavo G, Terenzio M (2014) Signalling endosomes in axonal transport: travel updates on the molecular highway. *Semin Cell Dev Biol* 27: 32 – 43

Simi A, Ibanez CF (2010) Assembly and activation of neurotrophic factor receptor complexes. *Dev Neurobiol* 70: 323 – 331

Sommerfeld MT, Schweigreiter R, Barde YA, Hoppe E (2000) Down-regulation of the neurotrophin receptor TrkB following ligand binding. Evidence for an involvement of the proteasome and differential regulation of TrkA and TrkB. *J Biol Chem* 275: 8982 – 8990

Steinberg F, Heesom KJ, Bass MD, Cullen PJ (2012) SNX17 protects integrins from degradation by sorting between lysosomal and recycling pathways. *J Cell Biol* 197: 219 – 230

Steinberg F, Gallon M, Winfield M, Thomas EC, Bell AJ, Heesom KJ, Tavare JM, Cullen PJ (2013) A global analysis of SNX27-retromer assembly and cargo specificity reveals a function in glucose and metal ion transport. *Nat Cell Biol* 15: 461 – 471

Teng KK, Felice S, Kim T, Hempstead BL (2010) Understanding proneurotrophin actions: recent advances and challenges. *Dev Neurobiol* 70: 350 – 359

Terenzio M, Golding M, Schiavo G (2014) SiRNA screen of ES cell-derived motor neurons identifies novel regulators of tetanus toxin and neurotrophin receptor trafficking. *Front Cell Neurosci* 8: 140

Voss AK, Thomas T, Gruss P (1998) Efficiency assessment of the gene trap approach. *Dev Dyn* 212: 171 – 180

Wade A, Thomas C, Kalmar B, Terenzio M, Garin J, Greensmith L, Schiavo G (2012) Activated leukocyte cell adhesion molecule modulates neurotrophin signaling. *J Neurochem* 121: 575 – 586

Wanschers BF, van de Vorstenbosch R, Schlager MA, Splinter D, Akhmanova A, Hoogenraad CC, Wieringa B, Fransen JA (2007) A role for the Rab6B Bicaudal-D1 interaction in retrograde transport in neuronal cells. *Exp Cell Res* 313: 3408 – 3420

Wichterle H, Lieberam I, Porter JA, Jessell TM (2002) Directed differentiation of embryonic stem cells into motor neurons. *Cell* 110: 385 – 397

Yacoubian TA, Lo DC (2000) Truncated and full-length TrkB receptors regulate distinct modes of dendritic growth. *Nat Neurosci* 3: 342 – 349

Yu T, Calvo L, Anta B, Lopez-Benito S, Lopez-Bellido R, Vicente-Garcia C, Tessarollo L, Rodriguez RE, Arevalo JC (2014) In vivo regulation of NGF-mediated functions by Nedd4-2 ubiquitination of TrkA. *J Neurosci* 34: 6098 – 6106

Zagrebelsky M, Holz A, Dechant G, Barde YA, Bonhoeffer T, Korte M (2005) The p75 neurotrophin receptor negatively modulates dendrite complexity and spine density in hippocampal neurons. *J Neurosci* 25: 9989 – 9999

